

AperTO - Archivio Istituzionale Open Access dell'Università di Torino

The unseen evidence of Reduced Ionicity: The elephant in (the) room temperature ionic liquids

This is the author's manuscript

Original Citation:

Availability:

This version is available <http://hdl.handle.net/2318/1800258> since 2022-02-28T13:09:44Z

Published version:

DOI:10.1016/j.molliq.2020.115069

Terms of use:

Open Access

Anyone can freely access the full text of works made available as "Open Access". Works made available under a Creative Commons license can be used according to the terms and conditions of said license. Use of all other works requires consent of the right holder (author or publisher) if not exempted from copyright protection by the applicable law.

(Article begins on next page)

1 The unseen evidence of Reduced Ionicity: the elephant in (the) room 2 temperature Ionic Liquids

3
4 Alessandro Mariani,^{*a,b,c} Matteo Bonomo,^{c,d} Xinpei Gao,^{a,b} Barbara Centrella,^{c,d} Alessandro Nucara,^e Roberto Buscaino,^d
5 Alessandro Barge,^f Nadia Barbero,^d Lorenzo Gontrani,^{c,g} and Stefano Passerini,^{*a,b}

6 ^aHelmholtz Institute Ulm (HIU), Helmholtzstrasse 11, 89081 Ulm, Germany.

7 ^bKarlsruhe Institute of Technology (KIT), P.O. Box 3640, 76021 Karlsruhe, Germany.

8 ^cDepartment of Chemistry, Sapienza University of Rome, P. le Aldo Moro 5, 00185 Rome, Italy

9 ^dDepartment of Chemistry and NIS Interdepartmental Centre and INSTM Reference Centre, University of Turin,
10 via Pietro Giuria 7, 10125 Turin, Italy

11 ^eDepartment of Physics, Sapienza University of Rome, P. le Aldo Moro, 5 00185, Rome, Italy

12 ^f Department of Drug Science and Technology, University of Turin, via Pietro Giuria 7, 10125 Turin, Italy

13 ^gDepartment of Industrial Engineering, University of Rome, Tor Vergata, Viale degli Ingegneri, I-00133 Rome, Italy

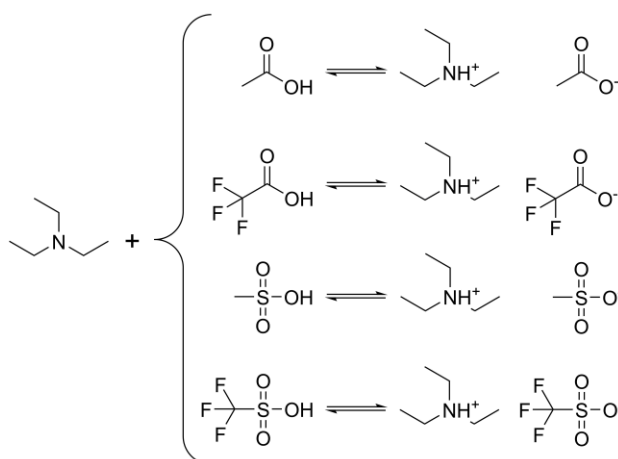
14 Abstract

15 The unambiguous quantification of the proton transfer in Protic Ionic Liquids (PILs) and its
16 differentiation from the concept of ionicity are still unsolved questions. Albeit researchers awfully
17 quickly treat them as synonyms, the two concepts are intrinsically different and imply a dramatic
18 modification in the expected chemical and physical properties of a PIL. Some attempts have been
19 made to shed light on this discrimination, but single-technique-based approaches fail in giving a
20 clear answer. Aiming at definitively figuring out the differentiation between proton transfer and
21 ionicity, we performed a multi-technique analysis (NMR, Raman, IR, thermal and electrochemical
22 analyses, among others). Indeed, thermal and spectroscopic analyses are employed to determine
23 the acid strength's role in ions' complete formation. To overcome the ambiguity between ionicity
24 and formation degree, we introduce a new paradigm where Reduced Ionicity accounts for both the
25 quantities mentioned above. The reduced ionicity directly affects the thermal stability, the phase
26 behavior, and the spectroscopic observations, resulting in particular features in NMR and vibrational
27 spectra. The combination of physical-chemical analyses and Pulsed-Gradient Spin-Echo (PGSE) NMR
28 allows determining the reduced ionicity (and not the ionicity, as reported so far) of the investigated
29 systems. In this context, being the proton transfer not quantitatively accessible directly, the reduced
30 ionicity of a reference series of triethylamine-based PILs is investigated through transport properties
31 as a function of temperature. Our findings point toward a substantial dependence of the reduced
32 ionicity by the acid strength and the anion's coordination power. Furthermore, some interesting
33 insights about the proton transfer are obtained, combining all the findings collected.

34 Introduction

35 Protic Ionic Liquids (PILs) are a sub-class of the nowadays widely studied ionic liquids[1–5] since they
36 follow the general definition given by Walden in 1914, *i.e.*, "water-free salts that are in liquid form
37 below 100 °C" [6]. A more rigorous definition is currently adopted as water-free organic salts
38 showing a melting point at temperatures below their decomposition. Ionic liquids have been
39 successfully applied in different fields ranging from sensors to solar cells and batteries, and they can
40 also be employed as lubricants in technological applications[7–15]. Indeed, interactions leading to

1 PILs formation are constituted by a subtle balance of "weak" forces (*e.g.*, Coulombic interactions,
 2 hydrogen bonding, cohesion, and dispersion forces). ILs are generally classified into two prominent
 3 families: protic ionic liquids and aprotic ionic liquids (AILs). The former family results from the proton
 4 transfer between two neutral species[16], while the AILs are formed by the interaction of two
 5 preformed ions that, once mixed, give rise to the liquid system. As highlighted in Scheme 1, the
 6 reaction forming PILs is an equilibrium reaction, meaning that the parent compounds may always
 7 exist together with the ionic species. This apparent weakness in terms of stability of the ionic species
 8 can be turned into an advantage. While most AILs have almost zero vapor pressure, PILs precursors
 9 generally have low boiling points, enabling their distillation thanks to the Le Châtelier's principle[17].
 10 Their ability to establish extended 3D hydrogen-bonded networks[18] gives rise to a series of
 11 exciting properties like enhanced proton mobility and peculiar solvation character as observed both
 12 experimentally[19–24] and by theoretical calculations[21,25,26]. PILs share morphologically similar
 13 hydrogen bond networks with water[27], although they differ in almost every aspect. The ease of
 14 preparation and the usually cheap precursors make them appealing materials for a wide range of
 15 applications[9]. Examples span from electrochemistry[28] to catalysis[29]; the latter also thanks to
 16 their ability to dissolve a wide variety of compounds[30–35]. As PILs form via an equilibrium
 17 reaction, "neat" protic ionic liquids are not usually achieved, but some acid and base will be present
 18 in the system. To minimize the fraction of parent compounds, the use of strong acids and bases
 19 certainly helps. In this work, we employed triethylamine (TEA) as a Brønsted base in combination
 20 with a family of acids offering growing Brønsted acidity, *i.e.*, acetic acid (HAc), trifluoroacetic acid
 21 (HTFA), methanesulfonic acid (mesylic acid, HMS) and trifluoromethanesulfonic acid (triflic acid,
 22 HTfO), adhering to Scheme 1.
 23



24 Scheme 1: Compounds discussed in this work. From top to bottom: Triethylammonium acetate; Tri-ethylammonium
 25 trifluoroacetate; Triethylammonium methanesulfonate; Triethylammonium trifluoro-methanesulfonate.

26
 27 However, regarding triethylammonium acetate, a two-phase liquid was always obtained
 28 despite the synthetic route adopted, although previous reports indicated the successful
 29 synthesis of this compound[36–38]. In particular, we found the lower phase to be a mixture
 30 of the product and acetic acid in the mole ratio 1:3. Indeed, ¹H-NMR analyses (data not
 31 shown) of the upper (colorless) and lower (brownish) phases suggest that the former, which

1 has the smallest volume, is almost entirely made up of trimethylamine with the PIL present
2 only in traces.

3 On the other hand, the lower and most abundant phase contains the final product and a
4 significant excess of acetic acid. It should be noticed that the preparation protocol followed
5 in the reports mentioned above [36–38] involved the distillation of the final product to
6 remove the solvent. We may suggest that the amine-rich phase was lost upon distillation,
7 resulting in the mixture of acetic acid and IL being misrecognized as a pure ionic liquid. In
8 fact, in other manuscripts, the formation of two phases has been reported[39]. Recently, it
9 was shown experimentally[40,41] and computationally[42] that the PIL is, indeed, not
10 formed when equimolar quantities of triethylamine and acetic acid are mixed.

11 In the following, only the PILs resulting from the reaction of triethylamine (TEA) with either
12 trifluoroacetic, mesylic, or triflic acid are considered because they form single-phase
13 products. The determination of the proton transfer is often overlooked and sometimes
14 confused with the ionicity of the system. The latter does not measure specifically the number
15 of ionic species in the system, but it is instead a value indicating how many free charge
16 carriers are present in the system. For an ionic liquid consisting of a cation A^+ and an anion
17 B^- , the following expression defines the ionicity I :

$$I = \frac{[A^-] + [B^+]}{[A^-] + [B^+] + [A^-B^+]} \quad (1)$$

19 where the square brackets indicate the concentration of the species comprised, and $[A^-B^+]$
20 indicates the concentration of close ion-pairs. In order to be rigorous, the activity of the
21 species should be used to calculate any thermodynamic quantity, but on first approximation,
22 the use of concentrations could be accepted. It immediately appears clear how any neutral
23 molecule is not included in the ionicity definition. In the case of protic ionic liquids, the cation
24 carries a net charge due to protonation; thus, we will use HB^+ to indicate the cation. The
25 subtle difference between the proton transfer and ionicity resides in the fact that the
26 experimentally accessible quantities (*vide infra*) commonly used to determine ionicity can
27 be decreased by three mostly independent factors: (i) the proton (back)transfer, (ii) the
28 charge transfer between ions, and (iii) the ion association. Spectroscopic approaches have
29 been proposed to quantify the proton transfer[43], but the method proposed relies on the
30 assumption that the solvation shells and dielectric constant of the systems stay unperturbed
31 upon changing the composition of the system, which is questionable. MacFarlane's group
32 extensively addressed the proton transfer topic[39,44,45], but always accounting for ΔpK_a
33 values, which are strictly meaningful only in aqueous systems. They also pointed to the
34 proton transfer's qualitative spectroscopic determination [44], but again overlooking the
35 different chemical environments experienced by the species in the Brønsted precursors and
36 the ILs. Ionicity and proton transfer cannot be used as synonyms, albeit directly
37 correlated[46]. The proton transfer (or Formation Degree, FD) is a thermodynamic quantity
38 indicating the fraction of the Brønsted precursors involved in the proton exchange reaction.
39 For a Brønsted acid (HA) reaction with a Brønsted base (B) to form the PIL $HB^+ A^-$, we have:

1

$$K_{PT} = \frac{[A^-] \cdot [HB^+]}{[HA] \cdot [B]} \quad (2)$$

$$FD = \frac{[A^-] + [HB^+] + [A^-HB^+]}{[A^-] + [HB^+] + [A^-HB^+] + [HA] + [B]} \quad (3)$$

2

3 where K_{PT} is the equilibrium constant for the proton transfer.

4 The concept of charge transfer refers to the evidence of ions with non-integer electric
5 charge[47–50]. Nevertheless, this effect, which is pivotal in aprotic ionic liquids[50,51],
6 contributes only marginally to the ionicity value when Protic Ionic Liquids are considered.
7 The charge transfer accounts for electron clouds sharing between ions (*i.e.*, negative charges
8 moving from one species to another); on the other hand, proton transfer (*i.e.*, positive
9 charges moving from one species to another) has a much more marked effect statistically
10 and also in absolute value.

11 Strictly speaking, the concept of ionicity refers to the number of "free" ions in solution, as
12 defined in Equation 1. Thus, the eventual formation of tight ion-pairs or the occurrence of
13 other intermolecular interactions will not directly influence the proton transfer but will have
14 a significant impact on system ionicity.

15 Triethylammonium triflate (TEATfO) and triethylammonium mesylate (TEAMS) have already
16 been thoroughly investigated by Ludwig *et al.* [23,52–54]. However, they mainly focused on
17 the spectroscopic characterization of these materials, simplistically assuming a complete
18 formation of the PILs. Albeit they achieved a very in-depth knowledge of the systems,
19 whether such systems are neat ILs or mixtures of ILs and their precursors is still undefined.
20 Indeed, the second option seems to be the most likely. For example, Davidowsky *et al.*[55]
21 investigated the ionicity of very similar systems (*i.e.*, TEA was replaced by diethyl-methyl
22 amine, DEMA), finding an interesting correlation between the proton affinity of the acid in
23 the gas phase and the PIL proton transfer: the lower the former, the higher the latter,
24 resulting in the following order for the proton transfer: HAc < HTFA < HMS < HTfO. However,
25 the ionicity of the DEMATfO was found to be as high as 0.61. We reasonably expect a higher
26 ionicity in TEATfO, being TEA a stronger Brønsted base than DEMA. A remarkable effort in
27 the proton transfer study in PILs has been made recently by Hasani *et al.* [56] employing ¹⁵N
28 NMR on a series of pyridine-based systems. They find a clear correlation between the
29 difference of Brønsted precursors' proton affinities and the chemical shift of TEA nitrogen
30 atom. Nevertheless, this approach does not return quantitative results, is limited to
31 "ammonium" PILs, and requires ¹⁵N labeled samples, which are substantially expensive.

32 Unfortunately, the proton transfer cannot be directly determined in practice. Many attempts
33 have been made to employ potentiometric methods[57–61]. However, albeit the authors
34 find reasonable correlations between proton transfer (*i.e.*, the number of neutral species in
35 the mixture) with the acid strength of the proton donor precursors, some points prevent us
36 from relying on this approach entirely:

37 (i) no matter the IL investigated, two typical trends are evidenced: an almost quantitative
38 proton transfer (related to a meager amount of neutral precursor) or an almost null proton

1 transfer (IL not formed), whereas intermediate situations seem not to be detectable with
2 this approach. (ii) The authors started from the assumption that a superacid (triflic acid,
3 triflimidic acid (HTFSI)) in an aqueous environment could be used to titrate the unreacted
4 base quantitatively. However, this assumption is not supported by experimental data
5 regarding triflic acid strength in pure ionic liquids. For example, Kanzaki *et al.* [57,60] show
6 how, in an IL, the H_3O^+ is a stronger acid than HNO_3 , whereas the opposite is true in an
7 aqueous environment. There is no evidence that HTfO or HTFSI are stronger acids than HNO_3
8 in the IL environment; thus, the proposed approach seems to be based on not universally
9 valid assumptions. (iii) Moreover, the employment of triflic acid [60] or triflimidic acid [57]
10 as a titration agent will lead to the formation of a ternary system in the investigated
11 environment. Taking as example EAN, when triflic/triflimidic acid is added, the system
12 becomes a mixture of EAN and EA-TfO/TFSI that could influence the linearity in the response
13 of the electrochemical measurements. Finally, (iv) The reported approaches neglect the
14 presence of water traces in the IL entirely. The latter's amount is calculated in the range of
15 50-100 ppm [57,60] for different ionic liquids corresponding to a mole percent in the range
16 of 4-8% if we consider EAN. Practically speaking, the contribution of water should be
17 considered at least when dealing with almost-completely-formed ILs: indeed, in these cases,
18 the concentration of H_2O is higher than the one of the unreacted ethylamine, and its basicity
19 could also be comparable if not higher (in IL environment) than the latter. If so, the titration
20 would involve two different species (H_2O and Et-NH_2), and the quantification of the amine
21 could be largely overestimated. The pioneering theoretical work of Ingenmey *et al.* [62]
22 makes use of Quantum Cluster Equilibrium Theory to obtain several thermodynamic
23 properties from two different PILs computationally. In that work, they find values for the
24 proton activities in fair agreement with the ones determined with the potentiometric
25 methods. On this basis, we aim to expand the current work by employing the experimental
26 and computational techniques abovementioned in a forthcoming paper.

27 For now, we focused on measuring the systems' ionicity but considering the incomplete
28 formation of the PILs while interpreting the results, *i.e.*, not only referring to ion association.
29 In this work, we qualitatively prove that a certain degree of the examined PILs is always
30 formed, no matter which acid is employed, through a spectroscopic approach. A first semi-
31 quantitative analysis of the PILs ionicity is done by considering the so-called Walden plot,
32 where the inverse of the viscosity is plotted against the molar conductivity[63]. Studies
33 [46,64] proposed an empirical factor to derive the ionicity of a solution directly from the
34 Walden plot: ΔW , the vertical distance from the bisector representing the ideal behavior,
35 and the system's value. Angell's approach has been proven to be trustworthy for simple
36 mixtures, but it mostly fails to predict the ionicity of more complicated systems such as
37 molten salts[65]. Concerning PILs, it could be considered a rule of thumb, whose validity
38 should be further confirmed by additional evidence.

39 Finally, we employ Pulsed-Gradient Spin-Echo (PGSE) NMR as an elegant approach to
40 measure self-diffusion coefficients (D) of the different species existing in a system[66,67].
41 This technique has been successfully employed in the study of pure ILs[68] and their mixtures
42 with salts[69,70] and solvents[71,72]. Back in 2007, however, Annat *et al.*[73] proved that

1 PGSE suffers from intrinsic internal gradients and can produce apparent diffusion
2 coefficients considerably varying (up to 20%) for different protons within a given molecule.
3 As a matter of fact, most common ILs are constituted by bulky ions. Thus, ^1H nuclei belonging
4 to the same species may experience somewhat different environments. Therefore, the
5 sizeable coupling will be present, and Brownian motion may not be sufficient to average out
6 the dipolar interactions. Therefore, they resorted to PG stimulated echo (PGSTE)
7 experiments, minimizing the issue. Currently, that method is the most exploited approach in
8 the field of ILs[74]. In the present case, however, it should be pointed out that, since both
9 the anion and the cation are relatively small, the classical PGSE sequence allows to obtain
10 consistent values (*i.e.*, the difference in the calculation of D using different ^1H nuclei of the
11 same molecule is well below the experimental error). The NMR-derived D values can be
12 inserted in the Nernst-Einstein (NE) equation to obtain the related conductivity.

13 By employing a set of the described complementary techniques, such as thermodynamic
14 measurements, vibrational spectroscopies, NMR spectroscopies, and computational
15 methods, we found that the usually adopted Nernst-Einstein-based approach is not
16 associated with the direct determination of the ionicity nor proton transfer. Nevertheless,
17 considering the diffusion coefficients of anions, cations, and acidic protons, a qualitative
18 conclusion is achieved. Our results prove out of any doubt that the correct interpretation of
19 experimental results is of vital importance to account for not-quantitative proton transfer in
20 protic ionic liquids. Finally, we introduce the new concept of Reduced Ionicity, a quantity
21 explicitly accounting for both ionicity (defined as non-paired ions in the system) and the
22 proton transfer extent.

23 **Results and discussion**

24 **Thermal characterization**

25 The DSC and TGA of the three formed compounds, collected to determine each PIL's
26 characteristic temperatures, are summarized in Table 1. First, the decomposition
27 temperature was determined to identify the temperature range in which the stability of the
28 system was not threatened. All following characterizations were planned accordingly. Figure
29 1 depicts the obtained results. Although some sources indicate the ILs decomposition to start
30 at the temperature where the mass loss is 3% (T'_d), a better approach consists of taking the
31 minimum of the TGA derivative curve as the decomposition temperature (T_d). For the sake
32 of comparison with literature data, we report the values obtained with both approaches in
33 Table 1, but the discussion will be based on the values obtained with the derivative method
34 (DTGA).

35 TFA anion appears to lead to the least stable PIL (TEATFA), with a T_d of 478 K. This is due to
36 the occurrence of the anion decarboxylation as previously reported at considerably higher
37 temperatures for the pure acid[75]. Such a decomposition path leads to the complete loss
38 of the sample, as witnessed by the absence of any residual mass.

39 TEAMS is more stable exhibiting T_d at 485 K. This PIL shows more than a single degradation
40 process, which can be ascribed to TEAMS' multi-step decomposition and its thermolysis

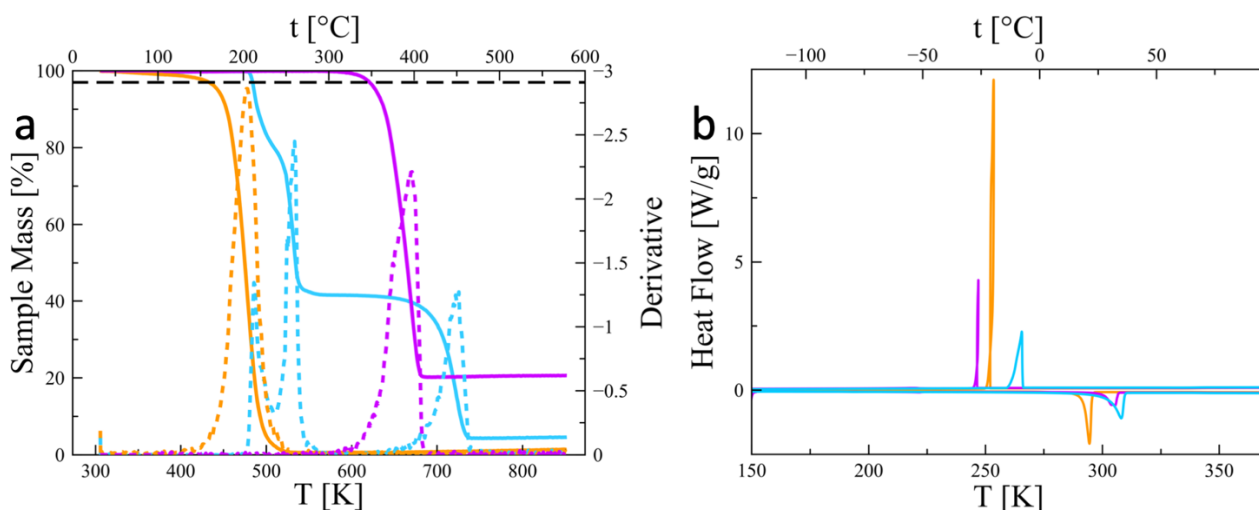
1 residuals. The most stable PIL is certainly TEATfO showing a T_d of 669 K. The analysis of the
 2 DTGA curve shows that TEATfO is also decomposing through a multi-step process similar to
 3 TEAMS. However, fluorination enhances the stability of the whole compound (with a residual
 4 mass at 800 °C higher than 20%). Indeed, TfO-based ILs are known to be thermally stable
 5 and are also used in fuel-cells[25,76]. The stability order interestingly follows the parent acid
 6 strength – TEATfO > TEAMS > TEATFA. Although some sources link the thermal stability to
 7 the extent of proton transfer[74,77,78], other evidence [79,80] highlighted that there is no
 8 direct correlation between the two properties, and caution is advised, especially when good
 9 leaving groups (*e.g.*, CO₂) are involved.

10 The phase transition temperatures of the PILs were investigated via DSC (Figure 1). At first
 11 glance, it appears that all three PILs can be extensively super-cooled, showing crystallization
 12 temperatures (T_c) well below their melting temperatures (T_m). The same was also observed
 13 while manipulating the samples for the analysis. All of them appeared solid at room
 14 temperature, but they melt after heating at 80 °C, remaining liquid upon storage at 20 °C for
 15 several weeks if left undisturbed in a vacuum desiccator.

16 According to the DSC curves in Figure 1b, TEATFA only shows T_c at 253 K and T_m at 294 K,
 17 with no sign of glass transition (T_g) in the examined range. TEAMS shows the T_g at 188 K in
 18 addition to the T_c at 266 K and T_m at 308 K, while TEATfO shows T_g , T_c , and T_m at 221 K,
 19 247 K, and 305 K, respectively.

20 The wide distribution of literature values[16,37,74,79–84] and the discrepancy with our
 21 findings could be explained considering the different water content in the range 1 ppm[16]
 22 - 2%_{mol}[74] for TEAMS and TEATfO, and 50 ppm[37] - 4200 ppm[79] for TEATFA. Sometimes,
 23 though, the water content is not even reported. Indeed, it is well known that even small
 24 differences in water content could have dramatic effects on IL properties, especially in
 25 PILs[85].

26



27 **Figure 1: (a) TGA (solid lines) and DTGA (dashed lines) collected (heating rate: 5 K min⁻¹) of TEAMS (cyan), TEATFA**
 28 **(orange), TEATfO (purple). The black dashed line corresponds to the 3% mass loss threshold. (b) DSC curves (heating rate:**
 29 **5 K min⁻¹) of TEAMS (cyan), TEATFA (orange), TEATfO (purple)**

30

1 Table 1: Comparison of thermal characterizations of this work (underlined) and literature. All values are expressed in
 2 Kelvin.

	T_c	T_m	T_g	T'_d	T_d
TEAMS	<u>265.53</u>	<u>308.03</u>	<u>187.68</u>	<u>484.25</u>	<u>485.52</u>
	241.55[81]	297.45[81]	194.25[81]		578.15[37]
	249.15[37]	306.15[37]	211.05[83]		491.15[74]
	242.15[74]	306.15[82]	176.65[16]		498.15[83]
	250.25[80]	298.15[74]	198.15[82]		542.85[16]
		290.55[83]			476.15[80]
		294.75[16]			563.15[82]
		306.25[80]			
TEATFA	<u>253.50</u>	<u>294.47</u>	--	<u>433.06</u>	<u>478.08</u>
	231.15[37]	275.15[37]	190.15[37]		463.15[37]
	231.75[79]	281.75[79]			459.45[79]
TEATfO	<u>246.97</u>	<u>305.34</u>	<u>221.26</u>	<u>620.56</u>	<u>657.55</u>
	253.15[37]	305.15[37]	215.15[37]		649.15[37]
	260.15[74]	299.15[74]	215.15[84]		595.15[74]
	243.85[80]	307.45[83]			631.15[83]
		306.35[80]			585.65[16]
		307.15[82]			588.55[80]
		309.15[84]			653.15[84]
					663.15[82]

3
 4 Anyhow, our results fit in the general trend already reported. Shmukler *et al.*[79] proposed a
 5 correlation between T_c and T_m for a series of triethylammonium-based PILs, including the three
 6 under investigation here, but we do not find anything similar. Again, the samples' different water
 7 content and thermal history could have a substantial effect on the observed thermal properties.

8 Conductivity and Viscosity

9 The study of PILs transport properties offers a deep insight into their nature; therefore,
 10 conductivity and viscosity measurements were carried out on all samples as a function of
 11 temperature (Figure 2). The experimental data clearly show Vogel-Tamman-Fulcher (VTF)
 12 behavior in both cases, markedly deviating from linearity in the Arrhenius plot ($\log \varphi$ vs.
 13 $1000/T$, in Figure S1). Thus, data were fitted with the equation:

$$\varphi(T) = \varphi_{\infty} \exp \left[-\frac{\xi_a^{\varphi}}{k_B(T - T_0)} \right] \quad (4)$$

14 where φ is either the conductivity (σ) or the viscosity (η), φ_{∞} is the value of that property at
 15 infinite temperature, ξ_a^{φ} is a parameter which is linked to the activation energy E_a^{φ} by $E_a^{\varphi} =$
 16 $|\xi_a^{\varphi}|$, k_B is the Boltzmann constant ($8.62 \cdot 10^{-5}$ eV K⁻¹), T is the absolute temperature, and T_0
 17 is the temperature of zero configurational entropy, often referred to as the "ideal glass-
 18 transition temperature". A comparison with literature data is given in Table 2, while Equation
 19 4 parameters are listed in Table 3. It is interesting to note how TEATFA is both the least
 20 viscous and the least conducive PIL. However, such a counter-intuitive behavior is difficult to
 21 justify only accounting for its low ionicity intended as "pronounced ion-pairing". If this were
 22 the case, the sample viscosity would have been higher due to the strong coulombic and

1 hydrogen-bonding forces between the ions. A more profound interpretation must consider
2 the IL's incomplete formation, resulting in a limited amount of charge carriers (explaining
3 the low conductivity), accompanied by a reduced viscosity coming from the unreacted
4 precursors (explaining the low viscosity). The presence in the TEATFA system of pure
5 triethylamine (0.345 mPa s at 25°C) and trifluoroacetic acid (0.813 mPa s at 25°C) is expected
6 to cause a net decrease in the viscosity, but at the expenses of available charged species
7 jeopardizing the conductivity. On the other hand, TEAMS appears to be by far the most
8 viscous PIL but displays higher conductivity than TEATFA. Once more, the degree of IL
9 formation plays a pivotal role in this PIL, too. Here, the surprisingly high viscosity is
10 undoubtedly caused by the more pronounced ion formation being mesylic acid stronger than
11 trifluoroacetic acid (*i.e.*, a higher proton transfer can be confidently assumed). As a
12 consequence, the conductivity is higher, although the viscosity reduces ion mobility. Finally,
13 TEATfO is, by a large margin, the most conductive PIL in the explored temperature range.
14 The low coordinating power of triflate, together with the strength of the triflic acid, makes
15 this result expected and in line with the literature[25,74,80,86]. Here, we could expect the
16 PIL to be nearly completely formed. Passing to the VTF space, E_a^σ and E_a^η values for TEATFA
17 are in excellent agreement with each other, suggesting that the conductivity in this system
18 is dominated by viscosity, and other effects, such as ion-pairing, are not significant. Once
19 again, this evidence hints at the incomplete formation of this particular IL. If the unreacted
20 precursors are in significant excess, then the ion-pairing is statistically limited since the
21 mixture would be more similar to a dilute salt solution rather than a proper ionic liquid.
22 Consequently, the activation energies for the viscous and conductive fluxes converge, *i.e.*,
23 once the charged species start moving, there is no additional energy required to break the
24 ion pairs activating the conductive flux. For the other two ILs, E_a^σ is lower than E_a^η suggesting
25 that for higher degrees of formation there is no need to activate the viscous flow to start the
26 conductivity. In an ion-rich system, there is no need for the ions to move to carry charges, as
27 they could make the charge "jump" from one site to another by merely changing their
28 solvation shells, *i.e.*, the hopping mechanism, with no need for viscous flow (As schematically
29 depicted in Figure S2 in Supporting Information). However, this effect should not be
30 confused with the Grotthuss mechanism, since no chemical reaction is involved in our case.
31 It is worth noting that the opposite is observed in AILs, in which stable ion clusters jeopardize
32 the conductivity. A widespread approach to qualitatively estimate the ionicity of the ionic
33 liquids is the so-called Walden plot, which correlates the logarithm of the molar conductivity
34 with the logarithm of the fluidity (η^{-1}). To obtain the molar conductivity, we extracted the ILs
35 molarity from density measurements (shown in Figure S3) and applied the relation:

$$\Lambda = \sigma \cdot \frac{\text{MW}}{\rho} \quad (5)$$

36 where Λ is the molar conductivity, ρ is the density expressed in g dm^{-3} , and MW is the sample
37 molecular weight. In the Walden plot, a reference ideal behavior line is represented by 1M
38 KCl, which is considered fully dissociated and, thus, 100% ionic. A second reference line is
39 usually displayed, assuming 10% ionization of the same 1M KCl solution. These references

1 appear to be wholly arbitrary[63,65] and often poorly discussed in the literature, with some
 2 groups reporting the line being "0.01M KCl", some reporting "0.1M KCl" and others the
 3 (correct) "1M KCl". Moreover, the aqueous KCl system was selected as a reference only
 4 because it displays a nice correlation between molar conductivity and fluidity. Here we use
 5 the unambiguous definition of the ideal behavior line to be "the bisector passing through
 6 the origin of the Walden plot" (*i.e.*, solution of Equation 6 with $\alpha=1$). For the 10% reference
 7 line, instead, we simply shift the ideal line down one order of magnitude on the y-axis, thus
 8 assuming that the conductivity is linearly dependent on the concentration, which might not
 9 be the case in ILs, but it helps to separate the Walden plot in well-defined regions. Systems
 10 lying in between these lines are qualitatively defined as "good ionic liquids". Should they fall
 11 above or below, then they would be considered super-ionic or poorly-ionic, respectively. In
 12 general, it is expected for any given system to obey the Walden rule[46]:

$$\Lambda\eta^\alpha = C \quad (6)$$

13 C is a temperature-dependent constant, and α is called the decoupling constant, which
 14 corresponds to the Walden plot's slope. The vertical distance between the ideal line and the
 15 examined system is called ΔW . Applying[36] the relation:

$$I_W = 10^{-\Delta W} = 10^{-\log(\Lambda/\Lambda_r)} = \frac{\Lambda_r}{\Lambda} \quad (7)$$

16 where Λ and Λ_r are the molar conductivity of the sample and the reference line, respectively,
 17 it is possible to estimate the Walden ionicity (I_W) of the system. From Equations 6 and 7, it
 18 appears evident that in the ideal case $\alpha=1$ and $\Delta W=0$, therefore we consider this specific
 19 case as our reference in the Walden plot. The results for the three PILs herein investigated
 20 are reported in Figure 2 and Table 4. All PILs lie below the ideal line, with TEATFA being just
 21 under the 10% I_W reference line, *i.e.*, it is classified as a poor-ionic liquid, which is in complete
 22 agreement with our previous suggestion of a scarcely formed PIL. The other two PILs lie in
 23 between the two reference lines, thus behaving as good-ionic liquids, with TEATfO being the
 24 closest to the reference 100% dissociation line. On a more quantitative analysis, through the
 25 ΔW values and Equation 7, the Walden ionicity values are obtained and reported in Table 4.
 26 As expected, I_W values follow the order TEATfO>TEAMS>TEATFA. Some groups suggested a
 27 correlation between the Walden ionicity of protic ionic liquids and the ΔpK_a of the Brønsted
 28 precursors[43,64,77]. While this approach yields consistent results, it must be considered
 29 contingent because pK_a values are meaningful only in water (and in a few other solvents).
 30 Angell, though, has shown[87] how ΔpK_a is undoubtedly a valid rule-of-thumb to rationalize
 31 qualitative results such as ΔW values. The pK_a values for the precursors used in this work
 32 were found in the literature[88–91] and conveniently reported in Table S1. From a physical
 33 point of view, ΔpK_a is related to the free energy of the proton transfer from the acid to the
 34 base through:

$$\Delta G^0 = -RT \Delta \ln K_a = -2.303 RT \Delta pK_a \quad (8)$$

1 where R is the gas constant. It must be clear that Equation 8 is strictly valid only if the proton
 2 transfer happens in a 1M aqueous solution, as also specified by Angell himself[16]. The
 3 results obtained for our systems are reported in Table 4. A markedly negative free energy is
 4 found for all the three systems, hinting at a quantitative proton transfer, in open
 5 contradiction with all the other experimental results. We can, therefore, conclude that this
 6 approach is not giving reliable information on the considered PILs. The same is true
 7 considering the hypothetical protic ionic liquid triethylammonium acetate, with a ΔpK_a of ~ 6 .
 8 By applying Equation 8, a $\Delta G^0 = -34.3 \text{ kJ mol}^{-1}$ is obtained at room temperature, which points
 9 toward a quantitative proton transfer. On the other hand, the reaction does not
 10 quantitatively occur in reality, as mentioned earlier. Yoshizawa *et al.* proposed that a
 11 $\Delta pK_a > 10$ is required for complete proton transfer[64], which would rule out
 12 triethylammonium acetate, but would consider TEATFA a completely formed PIL, which is
 13 also not the case (*vide infra*).

14 As pointed out by Davidowski and coworkers[55], proton affinity differences (ΔPA) are more
 15 reliable than ΔpK_a to discuss Walden ionicity in pure ionic liquids. DFT calculations in the gas
 16 phase could return the proton affinity value for every protonated/non-protonated pair
 17 discussed[92]. The proton affinities for the PILs herein investigated are reported in Table S2,
 18 while the ΔPA values are listed in Table 4. Interestingly, the ΔPA for triethylammonium
 19 acetate is $\sim 500 \text{ kJ mol}^{-1}$, in agreement with the experimentally observed non-quantitative
 20 formation of the ionic liquid.

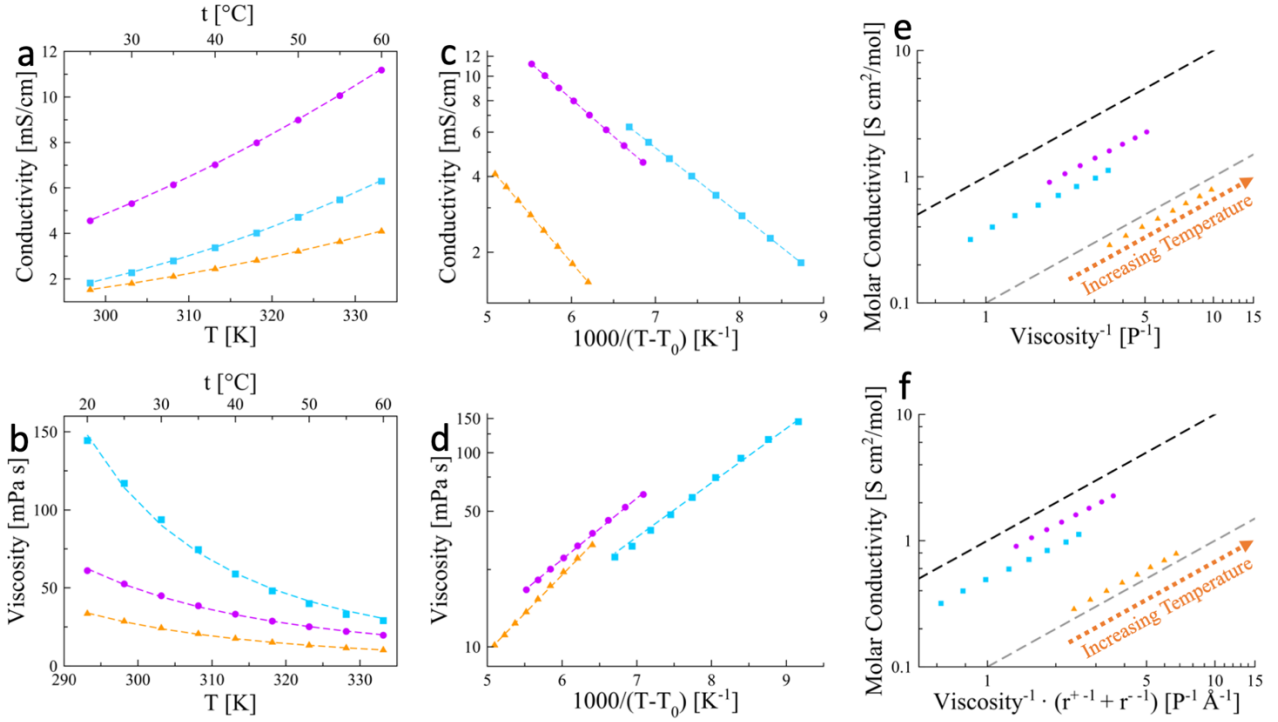
21 A useful correction to the Walden plot was introduced by Bonhôte *et al.* [93] and then re-
 22 proposed by Abbott and MacFarlane [46,94]. It is based on the role played by the ion size on
 23 diffusion, clearly highlighted in the Stokes-Einstein equation (Equation 9). They introduced a
 24 correction factor ζ for the viscosity explicitly accounting for the ion sizes (Equation 10), and
 25 then use $\log(\zeta\eta^{-1})$ in the Walden plot. Moreover, Equation 6 can be expressed as Equation
 26 11[46], explicitly showing the ion-size dependency of the Walden rule.

27

28 *Table 2: Conductivity [mS cm^{-1}] and viscosity [mPa s]. Data in this work (underlined) and in literature at 25 °C. Other*
 29 *temperatures and water content in brackets.*

TEAMS	TEATFA	TEATfo
Conductivity		
<u>1.84 (76 ppm)</u>	<u>1.52 (52 ppm)</u>	<u>4.55 (61 ppm)</u>
1.91 (100 ppm)[81]	2.45 (420 ppm)[79]	27.6 (120 °C) (N/A)[83]
2.03 (2% _{mol})[74]		4.79 (2% _{mol})[74]
16.3 (120 °C) (N/A)[83]		
Viscosity		
<u>117.0 (76 ppm)</u>	<u>28.6 (52 ppm)</u>	<u>52.5 (61 ppm)</u>
94 (810 ppm)[80]		56 (500 ppm)[80]

30



1 **Figure 2: Conductivity (a) and viscosity (b) as a function of temperature. Panels (c) and (d) show the VTF plots of the**
 2 **same quantities, respectively. Data points (symbols), VTF fit (dashed lines). Walden plot (e) and Rii-corrected Walden**
 3 **plot (f). Reference lines for 100% dissociation (black) and 10% dissociation (grey). TEAMS (cyan squares), TEATFA (orange**
 4 **triangles), TEATfO (purple circles).**

5
 6 **Table 3: VTF fitting derived parameters**

PIL	Conductivity		
	σ_{∞} [mS cm ⁻¹]	E_a^{σ} [10 ⁻² eV]	T_0^{σ} [K]
TEAMS	360±1	5.21±0.08	184±1
TEATFA	390±2	7.7±0.2	137±2
TEATfO	470±2	5.8±0.1	152±2
PIL	Viscosity		
	η_{∞} [mPa s]	E_a^{η} [10 ⁻² eV]	T_0^{η} [K]
TEAMS	0.41±0.06	5.6±0.1	184.0±0.2
TEATFA	0.098±0.004	7.87±0.06	137.0±0.1
TEATfO	0.35±0.02	6.27±0.06	152.0±0.1

7

$$D_i = \frac{k_B T}{f \eta r_i} \quad (9)$$

$$\zeta = \frac{1}{r^+} + \frac{1}{r^-} \quad (10)$$

$$\Lambda \eta^{\alpha} = C \left(\frac{1}{r^+} + \frac{1}{r^-} \right) \quad (11)$$

8 In Equation 9, D_i and r_i are the diffusion coefficient and the hydrodynamic radius of the
 9 species i , respectively. The parameter f is a constant with a value of 4π for entirely slip
 10 boundaries and 6π for perfectly stick boundaries. In Equations 10 and 11, r^+ and r^- are the

1 hydrodynamic radii of the cation and the anion, respectively. By applying the ζ correction
2 factor, the result is a horizontal shift of the Walden plot points, usually leading to smaller
3 $\Delta W'$ values[46] compared to the same quantity derived without accounting for ionic radii
4 correction, as can be seen in Figure 2 and Table 4. The hydrodynamic radius of the ions was
5 obtained as reported elsewhere[95]. The use of Ångstroms as units for the ion radii is
6 completely arbitrary, but it should be noted that the same arbitrariness is found in the choice
7 of centimeters for the molar conductivity and inverse Poise for the fluidity. The Walden plot
8 is built as an empirical tool and, consequently, the most convenient units are adopted to
9 return reliable and meaningful information.

10 By choosing the set of units [$\text{S cm}^2 \text{ mol}^{-1}$] vs. [$\text{P}^{-1} \text{ Å}^{-1}$], the I_W values obtained by Equation 7
11 are in good agreement with the values obtained with diffusion coefficients and Nernst-
12 Einstein equation (*vide infra*). The similarities between the systems make the overall relative
13 order to stay the same for the uncorrected Walden plot. Some critical difference, though,
14 can be appreciated. Most notably, TEATFA now lies just above the 10% I_W threshold line,
15 obtaining the status of good-ionic liquid, with a Walden ionicity of 11.8% obtained by
16 Equation 7. As it will be more explicit in the following, the correction is capable of returning
17 more reliable information than the classic approach. The linear fitting of the experimental
18 data in the Walden plot readily yields α and $\log C$ (Equations 6 and 11), which are the slope
19 and the intercept of the fitted line, respectively. For the three studied PILs, the fitting
20 parameters are shown in Table 4. The value for α is the same, being the correction just a
21 horizontal shift. On the other hand, the intercepts are markedly different for the bare (C)
22 and corrected (C') plots.

23 Extrapolating the lines obtained by the fitting to $\eta^{-1}=0$ (*i.e.*, infinite viscosity) when both the axis in
24 the Walden plot are expressed in linear scale, one obtains the conductivity at infinite viscosity ($\Lambda_{\eta\infty}$
25 in Table 4), which can be interpreted as resulting from the purely hopping ion movement, being any
26 diffusion-driven conductivity wholly frozen. TEATFA shows the lowest $\Lambda_{\eta\infty}$ values by a large margin,
27 which is explained by the anion's geometry. It is meaningless to define a $\Lambda'_{\eta\infty}$ including the radii-
28 correction since the intercept at $\eta^{-1}=0$ is unaffected by any multiplicative correction on the x-axis.

29 TFA anion can build, in its direct surroundings, a 2D network of hydrogen bonds since the two
30 carboxylic oxygen atoms lie in the plane. On the other hand, the triflate and mesylate anions have
31 an additional oxygen atom pointing out of the plane, resulting in a potentially 3D hydrogen-bonded
32 network. Moreover, the negative charge delocalized on two oxygen atoms makes TFA the most
33 prone to form firmly bound ion pairs. In this landscape, the potential energy barrier for the hopping
34 is markedly lower for TEATfO and TEAMS. The observed difference between these two can also be
35 explained in terms of the coordinating character of the ions. However, the geometry and the
36 coordination character are not the only properties contributing to the different behaviors. The
37 proton transfer of the PILs is likely to play a pivotal role in all these observations. The same approach
38 applied to aprotic ionic liquids would remove the uncertainty on the composition, thus returning a
39 more solid base for further discussion.

40
41
42

1 Table 4: Walden plots-derived parameters and other ionicity indicators. Both ΔW and $\Delta W'$ are the one calculated at 25°
 2 C (the difference is minimal with other points)

	TEAMS	TEATFA	TEATfO
α	0.884	0.975	0.932
C [S cm ² mol ⁻¹]	0.372	0.085	0.499
C' [S cm ² mol ⁻¹]	0.490	0.122	0.693
$\Lambda_{\eta \infty}$ [S cm ² mol ⁻¹]	0.074	0.013	0.107
ΔW	0.426	1.078	0.24
I_w [%]	37.5	8.4	57.5
$\Delta W'$	0.322	0.928	0.183
$I_{w'}$ [%]	47.6	11.8	65.6
ΔpK_a	12.7	10.6	24.8
ΔG^0 [kJ mol ⁻¹]	-72.5	-60.5	-141.6
ΔPA [kJ mol ⁻¹]	381.8	388.9	298.3

3

4 Raman Spectroscopy

5 Qualitative insight into the nature of the interactions in bulk PILs is provided by Raman
 6 spectroscopy. The presence of specific functional groups in the compounds and the different
 7 symmetry of the precursor Brønsted acid and its anionic conjugated base could shed light on
 8 the composition of the three PILs. In order to have a reliable set of references, the spectra
 9 of the pure precursors, the 1M aqueous solutions of each acid potassium salt, and
 10 triethylammonium chloride were also collected. In this way, it is possible to obtain the
 11 experimental spectra of the single ions since the monoatomic counter-ions K⁺ and Cl⁻ have
 12 no vibrational contribution. The solutions were diluted enough to avoid strong coupling
 13 between the ions. The collected data are plotted in Figure 3.

14 The band assignment, performed with the aid of DFT calculations, is reported in Supporting
 15 Information along with the calculated spectra (Figure S4). The spectra of all PILs are very
 16 well reproduced by the superposition of those from the cation and the anion, as can be
 17 expected for fully formed ionic liquids. However, some characteristic bands are identified
 18 (see Table 5), which could differentiate between ions and precursors. It is interesting to note
 19 that the point group of symmetry changes only for the pairs HMS/MS⁻ and HTfO/TfO⁻ passing
 20 from C_s to the more symmetric C_{3v}. The HTFA/TFA⁻ pair is always in the C_s group, while
 21 TEA/HTEA⁺ is in C₃, regardless of the protonation. These small molecular symmetry changes
 22 generate little-to-none modifications of the selection rules for the system's active normal
 23 vibration modes. Nevertheless, for all the anions, a band emerging from the deprotonation
 24 is easily tracked to witness the IL formation. The proton transfer activates the anti-symmetric
 25 stretching modes of the carboxylic (~1435 cm⁻¹) and sulfonic (~1040 cm⁻¹) functional groups.
 26 Unfortunately, there is no signal coming unambiguously from the Brønsted precursors,
 27 which would have allowed a quantitative determination of the ILs' proton transfer.

28 Nonetheless, PILs are formed to some extent because of the anions' anti-symmetric stretching peak
 29 presence in the spectra of the samples. A closer look at the TEA/HTEA⁺ δ_{hch} mode peak (Figure S5),
 30 though, hints again to the not complete formation of TEAMS and TEATFA. This feature appears to
 31 be distinctly asymmetric for these two compounds, clearly showing a shoulder at lower

1 wavenumbers. Comparing the PIL spectra with those of pure triethylamine and the 1M solution of
2 triethylammonium chloride (Figure S5), it can be concluded that there is a non-negligible amount of
3 the precursor Brønsted base (and, consequently, the acid) which has not reacted and remained in
4 the system. These results correlate well with those from Infrared and NMR spectroscopies (*vide*
5 *infra*). Focusing on TEATFA, the ν_{CC} band between 770 cm^{-1} and 870 cm^{-1} is diagnostic of the
6 formation of the anion for acetate-based systems, as shown by Umebayashi *et al.*[22,24]
7 Specifically, in the case of dissociation, the signal is substantially red-shifted if compared to the pure
8 acid one. Figure S6 reports the specific Raman region for the TEATFA system. As reported earlier[22],
9 the fingerprint of unreacted acid is clearly observed in the spectra.

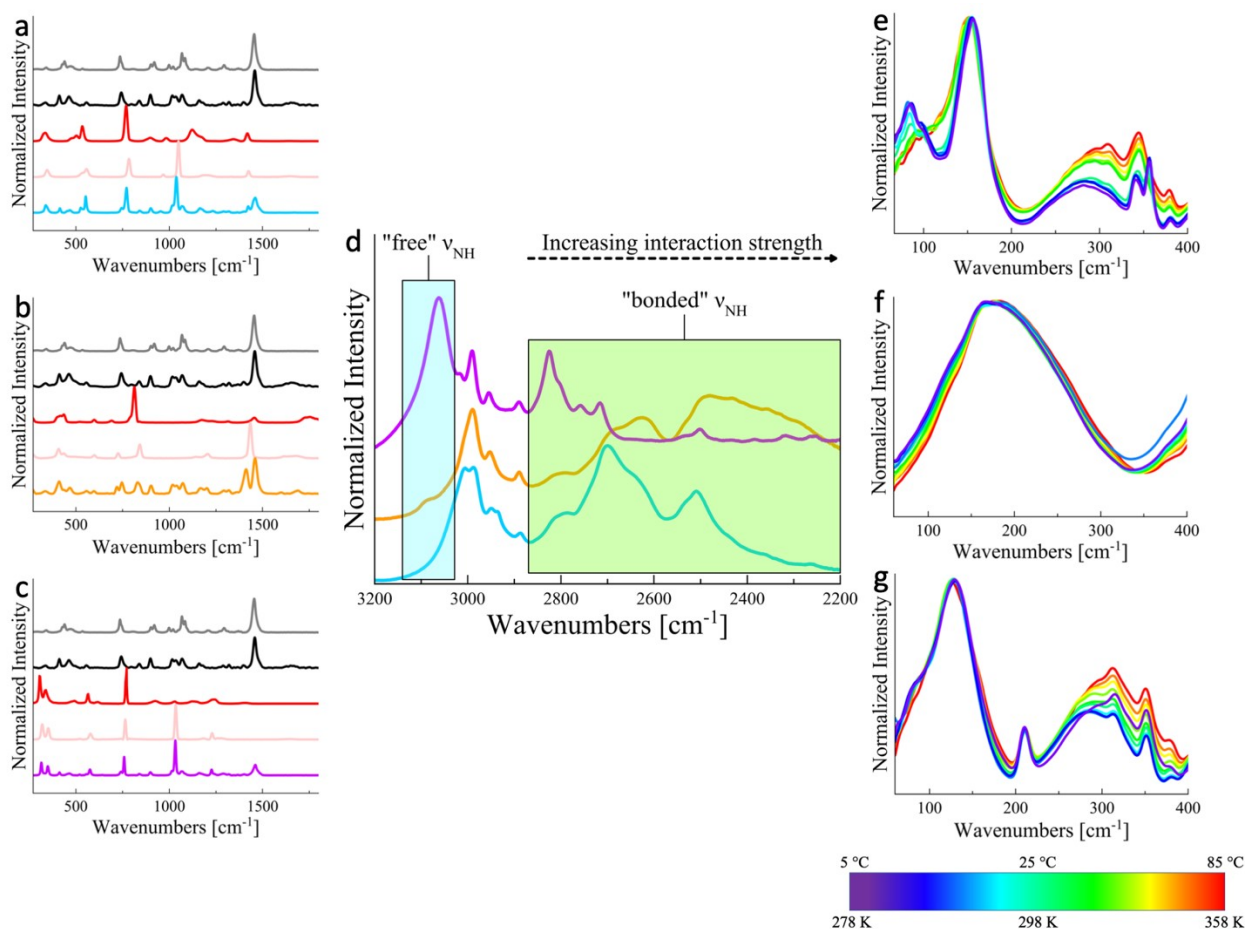
10 Albeit the signal in TEATFA is red-shifted compared to HTFA, it is at lower frequencies if
11 compared with the KTFA 1M solution.

12 In order to exclude the possible influence of different solvation shells and dielectric
13 constants, a system composed of TEATFA 67%_{vol} and HTFA 33%_{vol} was prepared, and its
14 Raman spectrum was collected. The comparison shows that the broad, asymmetric signal at
15 $\sim 830\text{ cm}^{-1}$ in TEATFA is due to unreacted acid rather than the anion. The pronounced blue-
16 shift compared to pure HTFA can be explained in terms of different dielectric constants and
17 solvation shells.

18 **Far Infrared Spectroscopy**

19 The Far Infrared (FIR) region of the vibrational spectra carries essential information regarding
20 the hydrogen bond features. In particular, the band between 100 and 200 cm^{-1} is
21 characteristic of the inter-species hydrogen bond stretching in PILs, as widely reported in the
22 literature[27,52,96–100]. TEAMS and TEATfO have already been studied by Ludwig *et al.*[53]
23 using FIR along with TEATFSI, including different deuteration degrees. These authors
24 correlated the interionic peak position with the hydrogen bond binding energy, but they also
25 state, "However, this relation was obtained by assuming that the full masses of anions and
26 cations are involved in the vibrational motion. If that is not the case, deviations from the
27 given relation can be expected", thus assuming that the PILs are completely formed, and the
28 band originates solely by the interaction between the ions. The evidence herein reported
29 are, however, point to a different direction, *i.e.*, a more complex system where different
30 hydrogen-bonding species coexist and potentially contribute to the observed FIR band. DFT
31 calculations show, indeed, that dimers of all three acids have active normal modes of
32 vibration in that region, arising from the anti-symmetric HB stretching (see Figure S7). Figure
33 3 reports the FIR spectra of TEAMS, TEATFA, and TEATfO collected as a function of
34 temperature.

35 Albeit the signal in TEATFA is red-shifted compared to HTFA, it is at lower frequencies if
36 compared with the KTFA 1M solution. In order to exclude the possible influence of different
37 solvation shells and dielectric constants, a system composed of TEATFA 67%_{vol} and HTFA
38 33%_{vol} was prepared, and its Raman spectrum was collected. The comparison shows that the
39 broad, asymmetric signal at $\sim 830\text{ cm}^{-1}$ in TEATFA is due to unreacted acid rather than the
40 anion.



1 **Figure 3: (a-c) Raman spectra at 25 °C of (a) TEAMS (cyan), TEATFA (orange), TEATfO (purple). In panels a-c (from top)**
 2 **pure triethylamine (grey), 1M aqueous triethylammonium chloride (black), pure corresponding acid (red), 1M aqueous**
 3 **potassium salt of the corresponding acid (pink). (d) X-H stretching region of Mid Infrared spectra at 25 °C. The boxes**
 4 **highlight specific stretching modes. From top TEATfO (purple), TEATFA (orange), TEAMS (cyan). (e-f) Far Infrared spectra**
 5 **as a function of temperature. (e) TEAMS, (f) TEATFA, (g) TEATfO. The temperature is indicated by the color bar.**

6
 7 **Table 5: Normal modes selected as a probe for ionic liquid formation.**

TEA/HTEA ⁺		HMS/MS ⁻		HTFA/TFA ⁻		HTfO/TfO ⁻	
cm ⁻¹	mode	cm ⁻¹	mode	cm ⁻¹	mode	cm ⁻¹	mode
1455	δ_{hch}	1050	$\nu^{\text{as}}_{\text{so}}$	1435	$\nu^{\text{as}}_{\text{co}}$	1035	$\nu^{\text{as}}_{\text{so}}$
--	--	--	--	830	ν_{cc}	--	--

8
 9 As reported above, a shift towards lower frequencies for increasing temperature is observed
 10 for TEAMS and TEATfO. The explanation given in the literature accounts for the weakening
 11 of the hydrogen bond as the temperature is increased. On the other hand, TEATFA shows
 12 the opposite behavior, *i.e.*, its broad band shifts toward higher frequencies upon heating.
 13 This counter-intuitive trend could find an explanation considering once more the not
 14 complete formation of this PIL. The trifluoroacetic acid is the weakest among the three
 15 tested herein. ¹H-NMR spectroscopy investigation of TEATFA (*vide infra*) clearly shows a peak

1 at ~11 ppm, which is more compatible with an acidic proton rather than an ammonium one.
2 It is reasonable to consider that a non-negligible amount of the acid is still in the system on
3 these bases. The heating of the IL below its decomposition temperature results in shifting
4 the equilibrium towards the formation of TEATFA. These results are seemingly in
5 disagreement with the literature [60,101], where an increased concentration of neutral
6 species is found in the gas phase upon heating of the ILs. It must be noticed, though, that
7 gas and liquid phases are intimately different. As a matter of fact, though, in the gas phase
8 a charged species is vastly less stable than in the liquid phase, being the density of oppositely
9 charged species (necessary to stabilize the ion) lower. Since the HB interactions in the PIL
10 are stronger than the one between neutral species, the increased number of ions in the
11 system explains the counter-intuitive blue-shift of the FIR band of this particular PIL upon
12 heating. This interpretation would also explain the broadness of the FIR signal for this PIL,
13 which results in the convolution of several different contributions, all active in a narrow
14 spectral window. It is also worth noting that for TEAMS and TEATfO, it is possible to recognize
15 the solid-to-liquid phase transition. Both PILs have a peak at $<100\text{ cm}^{-1}$ (for TEATfO it is only
16 a shoulder) at low temperatures, which gradually vanishes upon heating. For TEAMS, also
17 the peak at $\sim 360\text{ cm}^{-1}$, which is visible at lower temperatures, abruptly vanishes as the
18 system liquefies. These normal modes appear to be IR-active only in the solid-state, which
19 can be explained with a specific symmetry breaking. We are currently working to determine
20 the crystal structure of these compounds to clarify this and other observations. Others have
21 suggested[102] that the hydrogen-bond characteristic signal in PILs may be deconvoluted
22 into ion-ion mode and precursor-precursor mode. While it is conceptually a valid point,
23 caution is advised in applying such a simplistic approach. The presence of precursors in non-
24 negligible amounts would induce a plethora of different hydrogen-bonded pairs. Cation-
25 anion and acid-base interactions are positively contributing, but one must also consider the
26 effect of cation-base, cation-acid, anion-acid, and acid-acid even in the simplest case of a
27 single hydrogen-donor and a single hydrogen-acceptor. Not to mention possible collective
28 motions and (hindered) rotational modes that could impact this very low-frequency region
29 of the spectrum.

30 Infrared spectroscopy

31 We employed infrared spectroscopy to check for the formation of the ammonium functional
32 group because, in the specific case of triethylammonium cation, the N-H stretching (ν_{NH})
33 appears to be Raman-inactive[103] in our experiments (Figure S8). In the region around 3000 cm^{-1} ,
34 a plethora of active X-H stretching modes are active in the examined systems, but a
35 general trend is pointing towards a poorly-formed and highly-associated ionic liquid in the
36 case of TEATFA is emerging. In particular, the ν_{CH_2} signal is the highest frequency normal
37 mode found in pure triethylamine ($\sim 2975\text{ cm}^{-1}$), according to the NIST database[104]. In the
38 three PILs, the corresponding peak is clearly observed at $\sim 2988\text{ cm}^{-1}$, $\sim 2990\text{ cm}^{-1}$, and $\sim 2990\text{ cm}^{-1}$
39 for TEAMS, TEATFA, and TEATfO, respectively. Interestingly, an evident band splitting is
40 found for this vibrational mode for all three samples. The analysis of this feature is beyond
41 the scope of the present work, but a tentative interpretation is the presence of different

1 triethylammonium conformers in the system. The proton transfer on the nitrogen, though,
2 generates another additional signal at higher frequencies for TEATfO and, to a much minor
3 extent, TEATFA. This peak is attributed to poorly-interacting (or "free") ν_{NH} [80], whereas the
4 complex superposition of signals in the 2200-2850 cm^{-1} region is also assigned to ν_{NH} , but
5 with the proton interacting with the surroundings[80]. A strong endorsement for this
6 assignment comes from the complete absence of signals in both regions in the Raman
7 spectra. It is known that secondary amines[103] (and, by extension, tertiary ammonium ions)
8 show no ν_{NH} signals, having the N-H stretching only a very small Raman cross-section due to
9 the low change in the polarizability ellipsoid during the vibration. The strength of the
10 interaction is inversely proportional to the wavenumber of the vibrational mode. TEATfO
11 shows a clear, well-defined, and intense peak at $\sim 3062 \text{ cm}^{-1}$, and TEATFA has a low but
12 recognizable bump at $\sim 3088 \text{ cm}^{-1}$. TEAMS seems not to display the "free" ν_{NH} peak,
13 consistently with our other observations, which point towards strong ion-pairing in this
14 protic ionic liquid. Considering TEATfO, it is safe to say that the ionic liquid is extensively
15 formed and that most of it is not engaged in ion-pairing, as expected for the low-coordinating
16 triflate anion. Conversely, TEAMS appears to be also markedly formed, with most ions
17 hydrogen-bonded. TEATFA shows a minimum contribution for the "free" ν_{NH} , while a rich
18 population of vibrational modes is found in the "bonded" ν_{NH} region. It is worth noting that
19 N-H stretching modes usually have a high IR intensity, more pronounced than C-H modes.
20 The fact that in TEATFA the ν_{NH} broad signals only barely overcome the ν_{CH_2} points toward a
21 small ammonium population. These observations advise caution when dealing with protic
22 ionic liquids in assuming a priori a quantitative proton transfer.

23 NMR spectroscopy

24 Albeit NMR spectra could not unambiguously deduce quantitative information on the degree
25 of PILs' formation, some meaningful conclusions could be drawn. The collected ^1H , ^{13}C , and
26 ^{19}F NMR spectra are depicted in Figure 4.

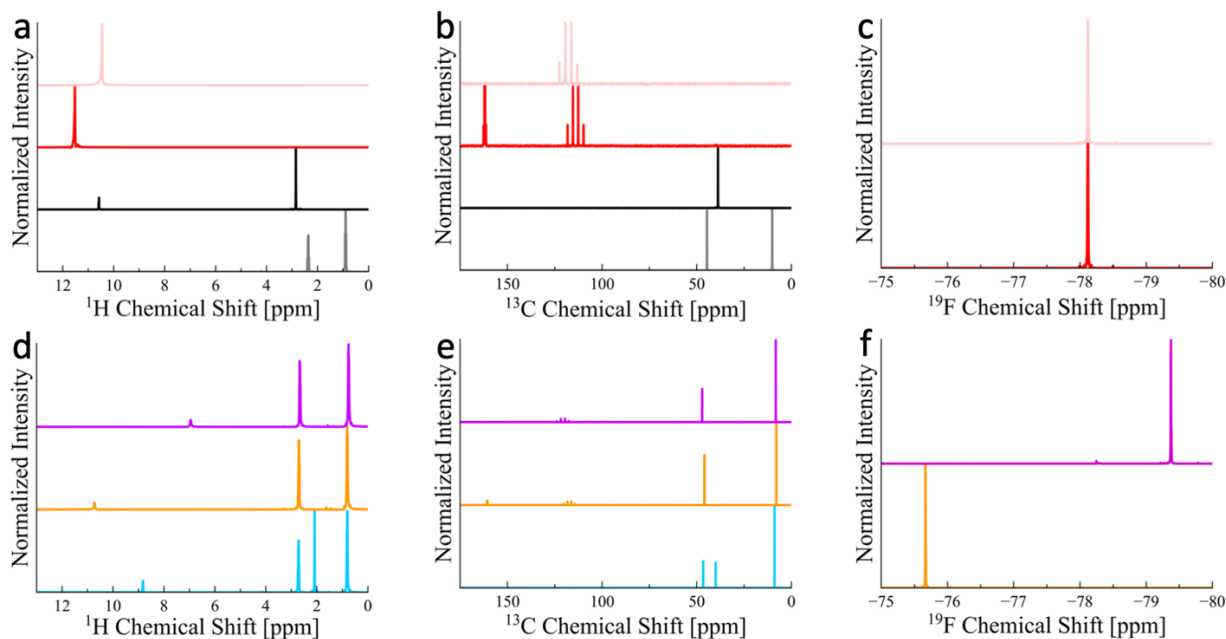
27 Along with the spectra of the prepared PILs, the respective Brønsted precursors were also
28 investigated to identify differences induced by the proton transfer. Interestingly,
29 Davidowsky *et al.* [55] analyzed diethyl-methylamine-based PILs correlating the proton
30 affinity of the acid with the chemical shift of the acidic proton: indeed, the higher the former,
31 the higher the latter. PA was preferred to pK_a since the latter is meaningful only in diluted
32 environments. The ^1H NMR spectra reported here show a similar trend: the downfield
33 shifted values here reported agree with the shielding effect of TEA. **On this basis, we found
34 an experimental confirmation of the actual proton transfer (*i.e.*, the formation of PILs),
35 which, unfortunately, does not give us any quantitative hint on the extent of proton transfer.**

36 The acid-to-base proton transfer also influences the chemical shift of $-\text{CH}_2-$ and $-\text{CH}_3$ groups
37 of the formed ammonium cation (HTEA^+) compared to pure TEA. Indeed, a shift at higher
38 ppm values is evidenced for the $-\text{CH}_2-$ group, whereas the resonance frequency of the $-\text{CH}_3$
39 group is only slightly influenced by the proton transfer, as it could be expected considering
40 the distance of the terminal methyl groups from the localized net positive charge on the
41 nitrogen atom. For the methylene group, the chemical shift follows the order TEATFA >

1 TEAMS > TEATfO, according to a previous report[55]. This trend seems to be counter-
2 intuitive, being the smallest shift brought about by the strongest acid. However, one should
3 consider that in a neat PIL, the cation is not isolated but rather surrounded (if not closely
4 paired) by anions, leading to a further modification of the resonance frequency experienced
5 by the methylene protons. The observed trend is in agreement with the anion coordination
6 power. The signal related to the methyl group of the anion in TEAMS slightly shifts towards
7 lower ppm values than pure HMS due to the acid "deprotonation". Regarding ^{13}C spectra,
8 the effect of proton transfer is reflected in the de-shielding of methylene carbon (in α
9 position to the protonation site), following the order TEATfO > TEAMS > TEATFA. The analysis
10 of ^{19}F is more puzzling, being the chemical shift is predominantly influenced by the
11 paramagnetic shielding rather than the diamagnetic one[105] in this case. Very
12 unexpectedly, the fluorine atom of both HTFA and HTfO resonates at an almost identical
13 frequency. A tentative explanation considers the sum of two factors: on the one hand, the
14 sulfonate group has a higher electron-withdrawing character; on the other, the HTFA⁺ forms
15 more persistent dimers implying a larger fraction of the negative charge delocalized on the
16 fluorine atoms. Once the PIL is formed, the ^{19}F signal of TEATfO shifts towards more negative
17 chemical shifts, whereas for the TEATFA the opposite behavior is observed.

18 As stated above, focusing on the mere chemical shift could be misleading; yet, some
19 interesting information could be extracted by comparing the PILs and the diluted aqueous
20 solutions of the corresponding acids (see Figure S9). It should be kept in mind that the acids
21 are entirely deprotonated if their molar fraction in water is lower than 0.4[106] (*i.e.*, 100
22 times more concentrated than our aqueous solution). Consequently, the obtained spectra
23 are representative of the anions and not the corresponding acids. ^{19}F spectrum of TEATfO is
24 almost entirely superimposed to that of TfO⁻, whereas the spectrum of TEATFA appears
25 0.8ppm down-shifted compared to TFA⁻. This inconsistency can be tentatively ascribed to
26 two different factors: (i) an incomplete formation of the PIL, being the ^{19}F signal a mediated
27 value between pure TEATFA and HTFA⁺; (ii) the instauration of intermolecular interactions
28 directly involving F atoms.

29 A verdict on this point (and more generally on NMR analyses) is far beyond the purpose of
30 the present work, but it will be discussed in the second part of this manuscript, where we
31 consider NMR to prove the formation of the PILs experimentally.



1 **Figure 4: NMR spectra collected injecting the sample and the deuterated solvent in two separate concentric**
 2 **tubes at 25 °C. The panels a-c refer to the Brønsted precursors, panels d-f refer to the ionic liquids. ¹H-NMR (a,**
 3 **d), ¹³C-NMR (b, e), ¹⁹F-NMR (c, f). From top triflic acid (pink), trifluoroacetic acid (red), mesylic acid (black),**
 4 **triethylamine (grey) (a-c); from top TEATfO (purple), TEATFA (orange), TEAMS (cyan) (d-f).**
 5

6 Ionicity vs. Reduced Ionicity

7 PGSE-NMR (Pulsed-Gradient Spin-Echo NMR) is the technique of choice when the
 8 investigated systems contain NMR-active nuclei. In our case, both the anion and cation of
 9 TEAMS are easily probed via ¹H-NMR. On the other hand, TEATfO and TEATFA are studied by
 10 means of ¹H-NMR (cation) and ¹⁹F-NMR (anion). The selected peak decay is fitted with the
 11 function of Wu *et al.*[67] reported in Equation 12:

$$\ln(I_g) = \ln(I_0) - (\gamma\delta g)^2 D \left(\Delta - \frac{\delta}{3} \right) \quad (12)$$

12 where I_g is the signal intensity when a field with gradient g is applied, I_0 is the signal intensity
 13 for $g=0$, γ is the gyromagnetic constant, Δ is the diffusion delay time, δ is the duration of the
 14 gradient pulse, and D is the desired self-diffusion coefficient.

15 The gradient is calibrated using a pure D₂O sample, where the diffusivity of HDO in D₂O is
 16 calibrated to $1.9 \cdot 10^5 \text{ cm}^2\text{s}^{-1}$ at 298 K. The diffusion coefficient of the cations and unreacted
 17 TEA, if present, are measured on both methyl (-CH₃) and methylene (-CH₂) peaks. These give
 18 roughly the same D value, and the values reported in Table 6 are averages of the two peaks.
 19 Concerning TEAMS, the D of the cation (and/or HMS) is measured on the methyl peak.
 20 Regarding TEATfO and TEATFA, being both the anions proton-free, the D values are
 21 measured for the fluorine peak by means of 2D ¹⁹F NMR. The determined self-diffusion
 22 coefficients as a function of temperature are listed in Table 6 (separated in anion and cation)
 23 and displayed in Figure 5 (summed).

1 The Stokes-Einstein relationship (SER, Equation 9) is widely employed to relate viscosity and
 2 diffusion coefficients. It has some severe limitations, though, which prevent its application
 3 in pure ionic liquids.

4 In particular, for SER to be valid (i) the investigated system must be a solution (*i.e.*, the
 5 solvent in significant excess of the solute), (ii) the radius of the solute must be substantially
 6 larger than the radius of the solvent, and (iii) the system must be dynamically homogeneous.
 7 On these bases, and considering the structural heterogeneity of many
 8 ILs[2,11,112,113,18,30,99,107–111], it is already clear that pure ionic liquids fail to meet all
 9 requirements.

10

11 Table 6: PGSE-NMR determined self-diffusion coefficients for the anions and cations as a function of
 12 temperature

t [K]	TEAMS [10 ⁻¹¹ m ² s ⁻¹]		TEATFA [10 ⁻¹¹ m ² s ⁻¹]		TEATfO [10 ⁻¹¹ m ² s ⁻¹]	
	Cation	Anion	Cation	Anion	Cation	Anion
298	1.11 ±0.01	1.47 ±0.02	2.47 ±0.03	1.63 ±0.02	2.00 ±0.02	1.17 ±0.01
303	1.26 ±0.02	1.59 ±0.06	2.57 ±0.05	2.08 ±0.05	2.14 ±0.02	1.41 ±0.06
308	1.42 ±0.03	1.82 ±0.05	2.99 ±0.06	2.5 ±0.2	2.35 ±0.03	1.8 ±0.1
313	1.68 ±0.04	1.94 ±0.07	3.30 ±0.06	2.8 ±0.4	2.64 ±0.04	2.1 ±0.1
318	1.99 ±0.05	2.26 ±0.09	3.40 ±0.09	3.2 ±0.4	2.71 ±0.05	2.4 ±0.2
323	2.43 ±0.07	2.63 ±0.07	3.70 ±0.09	3.7 ±0.3	2.95 ±0.06	2.7 ±0.2
328	2.70 ±0.08	2.9 ±0.1	3.96 ±0.09	4.1 ±0.4	3.22 ±0.08	3.0 ±0.3
333	2.8 ±0.1	3.0 ±0.1	4.1 ±0.1	4.4 ±0.4	3.49 ±0.08	3.3 ±0.3

13

14 Moreover, in the specific case of protic ionic liquids, one must also consider their different
 15 proton transfer, which also depends on the temperature. Therefore, an implicit boundary
 16 condition to the SER exists, *i.e.*, (iv) the ionic strength of the system must be constant with
 17 temperature. This condition is essential because a change in the PIL proton transfer would
 18 affect the radius of the moving species and enhance the dynamic heterogeneity by adding
 19 Coulombic interactions only in some areas of the system. The significant deviation of the
 20 investigated PILs from SER can be seen in Figure S10. Several corrections for SER have been
 21 proposed over the years, almost exclusively looking at different ways to define the
 22 hydrodynamic radius of the charged species[114]. As an example, Cheng-Li[115] correction
 23 (CLC) was explicitly developed for self-diffusion coefficients to overcome the (i) and (ii)
 24 limitations of SER. It considers the hydrodynamic radius to be:

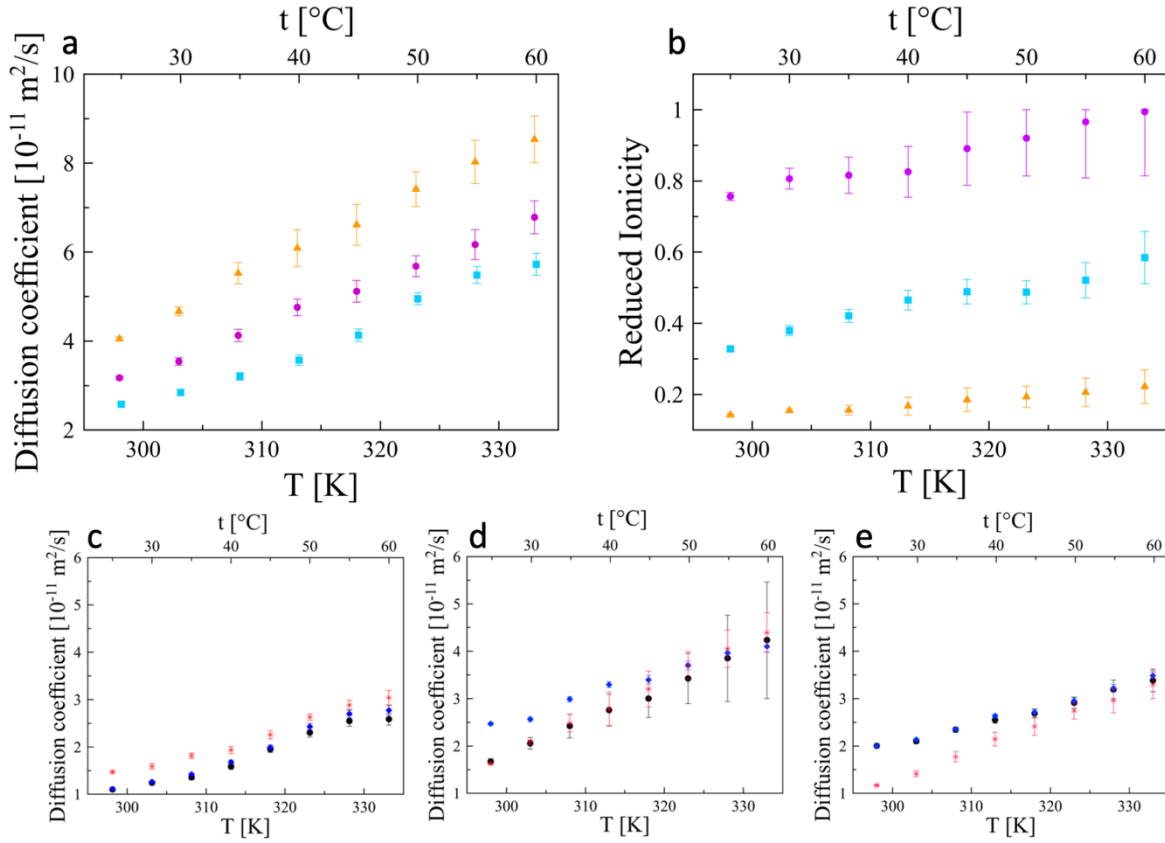
$$r_i = \sqrt[3]{\frac{V_m}{N_A}} \quad (13)$$

1 where V_m is the molar volume and N_A the Avogadro's number. While CLC returns good results
 2 for molecular liquids (usually within an error of 12%), it does not apply to ionic liquids
 3 because the molar volume depends on the specific configuration of the ion-pair, thus, in
 4 principle, being different for each one. Köddermann *et al.*[116] The leading cause for ILs
 5 deviations from SER is pointed at the dynamic heterogeneity, observing that if the IL is
 6 heavily diluted in a molecular liquid, the resulting system obeys SER. This finding is, though,
 7 expected because the system they obtained by dilution approached the requirements for
 8 SER to hold: (i) the new obtained system is a solution, (ii) the solvent used in their work was
 9 chloroform, which is markedly smaller than the IL investigated (namely, 1-ethyl-3-methyl-
 10 imidazolium bis (trifluoromethanesulphonyl) imide), (iii) the system is so diluted that any
 11 heterogeneity is averaged out. Their use of an aprotic ionic liquid also addressed the implicit
 12 fourth requirement on the proton transfer of the IL.
 13 As a different approach, we introduce an empirically derived temperature-dependent
 14 correction factor (β) obtained using the PGSE-NMR derived diffusion coefficients in SER.

$$\beta = \frac{k_B T}{6\pi \eta r_i D_{\text{NMR}}} \quad (14)$$

15 The correction factor β accounts for two physical phenomena of crucial importance in PILs:
 16 (i) the hydrodynamic radius of the diffusing species might significantly differ from those of
 17 the cations and anions themselves because of the possible aggregation driven by both
 18 Coulombic and aliphatic forces, and (ii) the partial formation of the ionic liquid generates
 19 regions with **locally different microscopic viscosity**, with low-viscosity domains where the
 20 Brønsted precursors are in excess existing along with high-viscosity parts where the IL is
 21 more concentrated. β values are shown in Table 7. As it appears clear from Equation 14, a
 22 system ideally follows SER for $\beta = 1$. If $\beta < 1$, the species in the system show a diffusion
 23 coefficient, which is larger than the one predicted by SER based on the macroscopic viscosity
 24 and the single-ion hydrodynamic radius. The opposite is true for $\beta > 1$.
 25 The effect of the correction parameter is then to adjust the quantity ηr_i to obtain effective
 26 viscosity and hydrodynamic radius. It is not possible to separate the two contributions
 27 because neither r_i nor the local viscosity are experimentally accessible. The obtained values
 28 show a marked dependence on the temperature, pointing towards the importance of the
 29 implicit requirement (iv). Moreover, especially for TEATFA, the higher the temperature, the
 30 larger than 1 is β , which rules out the hypothesis that changes in the effective r_i govern the
 31 deviation. In such a case, in fact, β should progressively become smaller (even smaller than
 32 one) upon increasing the temperature because clusters are expected to be destroyed at
 33 higher temperatures. Additionally, also the dynamic heterogeneity should be diminished by
 34 heating the system, but only if the sample composition remains constant at every
 35 temperature.

36



1 **Figure 5: (a) PGSE-NMR derived diffusion coefficients. The values are the sum of the anion and cation diffusion**
 2 **coefficients at the given temperature. TEAMS (cyan squares), TEATFA (orange triangles), TEATfO (purple circles).**
 3 **(b) Reduced Ionicity derived from the ratio Λ/Λ_{NE} . TEAMS (cyan squares), TEATFA (orange triangles), TEATfO**
 4 **(purple circles). (c-e) Comparison between the diffusion coefficients of the acidic proton (black circles), anions**
 5 **(red stars), and cations (blue diamonds). TEAMS (c), TEATFA (d), TEATfO (e).**

6

7 **Table 7: Temperature-dependent empirical correction factor for the Stokes-Einstein relationship**

	TEAMS		TEATFA		TEATfO	
t [K]	Cation	Anion	Cation	Anion	Cation	Anion
298	0.409	0.659	0.997	1.952	0.670	1.288
303	0.481	0.734	1.150	1.832	0.747	1.268
308	0.538	0.837	1.183	1.838	0.804	1.198
313	0.649	0.909	1.277	1.952	0.848	1.169
318	0.693	0.956	1.467	2.008	0.966	1.219
323	0.727	0.957	1.561	2.017	1.031	1.246
328	0.815	1.057	1.702	2.149	1.090	1.332
333	0.892	1.189	1.884	2.271	1.149	1.365

8

9 In our case, the proton transfer of the IL likely changes, generating more ions, which are
 10 responsible for more substantial viscosity variations. By plugging the PGSE-NMR derived
 11 diffusion coefficients in the Nernst-Einstein relationship (Equation 15), it is possible to

1 calculate the limiting molar conductivity, *i.e.*, the theoretical conductivity that a system
2 would have if all the moving species were carrying a net electric charge.

$$\Lambda_{NE} = \frac{N_A e_0^2}{k_B T} \cdot (D^+ + D^-) \quad (15)$$

3 In Equation 15, Λ_{NE} is the theoretical molar conductivity. D^+ and D^- are the diffusion
4 coefficients of the cation and the anion, respectively. Following the definition of Λ_{NE} , the
5 ratio Λ/Λ_{NE} is a measure of the ionicity of the system. It should be once more clarified that
6 the term "ionicity" for protic ionic liquids is ambiguous. Indeed, for aprotic ionic liquids, the
7 term is used to address the degree of dissociation, *i.e.*, is a measure of the ion-pairing
8 (Equation 1). For PILs, the scenario is more complicated because the proton transfer also
9 contributes to the "loss" of ion conductivity, resulting in a smaller Λ/Λ_{NE} ratio.

10 Based on all the experimental and theoretical evidence above, and to stop the dangerous
11 confusion between ionicity and proton transfer/formation degree in protic ionic liquids, we
12 propose the adoption of new terminology, introducing the concept of "Reduced Ionicity" (ι)
13 which is directly linked to both I and FD . It is possible to express ι as a function of the
14 concentration of all the species in the system, similarly to Equations 1 and 3:

$$\iota = \frac{[A^-] + [HB^+]}{[A^-] + [HB^+] + [A^-HB^+] + [HA] + [B]} \quad (16)$$

16
17 By recognizing that $[A^-]=[HB^+]$ and that $[HA]=[B]$, it is possible to combine Equations 1, 2, and
18 16 to obtain a direct relationship between I and ι :

$$\iota^{-1} = I^{-1} \cdot K_{PT}^{-1/2} \quad (17)$$

20
21 It directly follows that, in general, for any ionic system regardless of its nature (*e.g.*, aprotic
22 IL, protic IL, molten salt, aqueous solutions):

$$\frac{\Lambda}{\Lambda_{NE}} = \iota \quad (18)$$

23 contrary to what is usually reported in the literature, where the Λ/Λ_{NE} ratio is referred to as
24 the ionicity of the system. Indeed, it should be clear that Equation 16 holds even if all the
25 protonated species (HB^+ , A^-HB^+ , and HA) are exchanged with their aprotic counter-parts (B^+ ,
26 A^-B^+ , A). Equation 18 returns the ionicity only if the formation degree of the ionic species is
27 1, *i.e.*, $[HA]=[B]=0$, or $[A]=[B]=0$, which is the same for aprotic ionic substances.
28 Consequently, for PILs the term "ionicity" should not be used as it currently is because of the
29 possible incomplete proton transfer (*i.e.*, formation degree), and the more general reduced
30 ionicity should be used instead. By comparing Equations 1, 3, and 16 it is clear that FD is
31 always higher than (or, at least, equal to) the reduced ionicity value, but the same is not true
32 for ionicity. It is important noting the relationships in Equation 19.

33

$$\begin{cases} I \geq \iota \\ FD \geq \iota \end{cases} \quad (19)$$

1
2
3
4
5
6
7
8
9
10
11
12
13
14
15
16
17
18
19
20
21
22
23
24
25
26
27
28
29
30
31
32
33
34
35
36
37
38
39
40

The latter expression highlights why we adopted the term “reduced ionicity”, and shows how ι is a property fundamentally different from both I and FD . For example, in the case of a hypothetical PIL with $FD \ll 1$ (e.g., TEAAc), it is quite possible that its ionicity (as defined in Equation 1) would be close to 1, because of the high dilution of the ions in the Brønsted precursors. On the other hand, some PILs with strongly coordinating ions (e.g., chloride) could have $I \ll 1$ but FD (Equation 3) approaching 1. Both the systems in the examples would have $\iota \ll 1$ (Equation 16), and a deeper insight on the system is needed to identify the reasons behind the observed value obtained by the Λ/Λ_{NE} ratio.

The results of this approach applied to the three PILs studied here are reported in Figure 5. For all the presented PILs, the reduced ionicity increases with the temperature, which is expected considering both the breaking of ion-pairs and the enhanced formation of ions themselves. As mentioned above, these values result from both paired ions and neutral molecules in the system, and a quantification of their relative weight is not possible only based on the obtained reduced ionicity values.

Nevertheless, it is worth pointing to a possible solution to this seemingly insuperable *impasse*. As shown above, MIR spectroscopy shows two distinct signals for “bonded” and “free” ν_{NH} , thus offering a chance to obtain the ionicity of the system in line with its standard definition of non-paired ions in the system. In the three proposed examples, though, the “bonded” ν_{NH} region is too complex to attempt a reliable quantification. We will give more insight into this direction in a forthcoming paper.

One final insight, and definitive proof of the incomplete formation of TEATFA, is granted by a closer look at the diffusion coefficient trends. PGSE-NMR enables obtaining the diffusion coefficients of whatever has a suitable NMR signal, meaning that any peak can be followed to determine the diffusion coefficient of the associated species. In Table 6, the coefficients for anions and cations are reported for all the PILs herein investigated. These values are compared in Figure 5, with the diffusion coefficient of the acidic proton, which always shows a clear peak in the 1H -NMR of all the examined PILs. From Figure 5, it appears clear that the acidic proton diffuses bound to the amine in TEAMS and TEATfO, suggesting that the amine is the proton carrier, *i.e.*, the acid is deprotonated. Such a piece of evidence supports the substantial proton transfer in these two PILs. On the other hand, in TEATFA the proton essentially diffused with the CF_3 group, meaning that the acid is still mostly present in the system, confirming the incomplete proton transfer. At higher temperatures, the error bars for the acidic proton in TEATFA become too wide to give a robust interpretation of where the proton is. Such error bars could be seen as a hint to the increasing uncertainty on the proton position, which, at higher temperatures, can jump from the acid to the base more efficiently, increasing the IL proton transfer. All these pieces of evidence point at TEATFA being mainly composed of neutral species, TEATfO being a proper ionic liquid, and TEAMS being half-a-way between these two extremes. In this context, the reader is kindly invited to note how the superimposition of the ionicity concept with the one of proton transfer could

1 be safely done just for TEATfO, whereas other experiments are required to completely rule
2 out the formation of tough ion-pairs in both TEATFA and TEAMS. However, it is interesting
3 to note how the reduced ionicity values obtained in this rigorous way are in fair agreement
4 with those extracted by the radii-corrected Walden plot, suggesting that tool as a reliable
5 source of reduced ionicity values when PGSE-NMR cannot be used, even if with severe
6 limitations[65].

7 **Conclusions**

8 To summarize, we reported the characterization of thermal, transport, and spectroscopic
9 properties of three (plus one) triethylammonium-based protic ionic liquids with anions
10 originated from acids of different strengths. This series was chosen as a proof of concept to
11 discuss the intricate interplay between ionicity and proton transfer. The latter two concepts
12 are too often confused with each other, and the effective degree of proton transfer is too
13 easily overlooked, being considered quantitative. In this context, we aimed to investigate
14 these PILs by means of different approaches to shed light on the ionicity/proton transfer
15 interplay. We introduced the innovative concept of Reduced Ionicity for this scope and to
16 end the ambiguity between ionicity and formation degree, accounting for both the
17 phenomena. This quantity, and not the properly said ionicity, is what is obtained with the
18 Λ/Λ_{NE} ratio (Equation 18).

19 Using several complementary techniques, we have demonstrated how the proton transfer
20 in PILs is not always quantitative. The thermal stability follows the acid strength, with TEATfO
21 being the most stable. On the other hand, the relatively low stability of TEATFA is due to the
22 possible decarboxylation of the acid, which results in rapid evaporation of the whole
23 compound. All the spectroscopy techniques used hint at the incomplete formation of
24 TEATFA, but none of them was adequate to quantify the proton transfer. Nevertheless, the
25 overall picture given by NMR and vibrational spectroscopies returns the information that at
26 least some ionic liquid is formed in all the cases (Raman), that the degree of formation
27 follows the order TEATfO>TEAMS>TEATFA (NMR), and that raising the temperature below
28 the decomposition point increases the number of ionic species (FIR). MIR returns some
29 (unexpected) concrete direct evidence of (i) the poor proton transfer in TEATFA (displaying
30 only faint signals for the characteristic ν_{NH} vibrational modes), (ii) the sizeable proton transfer
31 in TEATfO (intense peak of the characteristic ν_{NH} vibrational modes) and (iii) the meaningful
32 aggregation experimented by TEAMS (ν_{NH} vibrational modes shifted toward lower
33 wavenumbers). In order to obtain complementary evidence towards further enlightenment
34 of proton transfer degree, the Walden plot remains a vital rule-of-thumb to classify these
35 materials. However, the radii-based correction factor is confirmed to improve the reliability
36 of Walden ionicity estimation vastly. In this regard, it should be noted how the Walden
37 ionicity approximates the reduced ionicity and not the ionicity itself. The Walden ionicity
38 calculated by the radius-corrected Walden Plot reasonably correlates with those measured
39 by the more conventional and reliable approach based on comparing the experimental and
40 Nernst-Einstein-derived conductivities. Overall, TEATfO can be considered a wholly-formed
41 PIL (*i.e.*, $\iota = I = FD = 1$ in the limit of relatively high temperatures). At the same time, a

1 qualitative consideration can be drawn concerning TEAMS and TEATFA, having reduced
2 ionicity values close to 0.6 and 0.2, respectively, at room temperature. While the values of
3 diffusion and viscosity for TEAMS are compatible with a low reduced ionicity solely
4 determined by ion-pairing, as firmly supported by the MIR spectra, the same is unlikely for
5 TEATFA, for which we propose a substantial influence of the incomplete proton transfer. This
6 conclusion is strongly supported by all the spectroscopic techniques used, particularly with
7 MIR and the 1:2_{vol} acid:PIL Raman spectra, and by the fact that the acidic proton clearly
8 diffuses with the trifluoroacetic species in the PGSE-NMR experiment. Very interestingly, the
9 diffusion coefficients calculated from the NMR analyses do not obey the Stoke-Einstein
10 relation nor any of the radii-correction terms proposed over time. Thus, we contextually
11 proposed an empirical correction factor, β , which accounts for local viscosity fluctuations
12 and hydrodynamic radii changes. It should be pointed out that, albeit a definitive
13 determination of ionicity and proton transfer was achieved only for TEATfO, we are
14 confident that, quoting Agatha Christie, (more than) *three coincidences are a proof*: TEAMS
15 has an almost quantitative proton transfer, but its reduced ionicity is jeopardized by ion-
16 pairs formation, while TEATFA experimented a very low proton transfer being also prone to
17 associating in ion clusters. In general, an IL can be considered pure if it is composed of at
18 least 99%_w of ions [117]. In the presented cases, only TEATfO and possibly TEAMS satisfy this
19 criterion, with TEATFA most probably being a mixture of PIL and Brønsted precursors.
20 This work clearly shows that more (and different) approaches are required to shed light on
21 the interplay between ionicity and proton transfer, a key topic in determining PILs' features,
22 too often overlooked in the literature.

23 **Methods**

24 **Materials**

25 All materials were purchased at the highest degree of purity available and employed without
26 further purification. Triethylamine $\geq 99.8\%$ Merck, Triflic acid $\geq 99.5\%$ T&J Chemicals, Mesylic
27 acid $\geq 99.5\%$ Merck, Trifluoroacetic acid 100% VWR Chemicals, Acetic acid $\geq 99.99\%$ Sigma
28 Aldrich.

29 **Synthesis of the Ionic Liquids**

30 The three PILs were prepared according to the following procedure. Triethylamine was
31 poured into an ice-bath cooled, three-neck flask under dry nitrogen flow (1ml/min). A
32 stoichiometric amount of the acid was then added dropwise under vigorous stirring over
33 three hours. The flask was then removed from the cooling but left under stirring at room
34 temperature over 12-16 hours. The final water content, determined by Karl-Fischer
35 coulometric titration, was found in the range of 50-80 ppm for all three PILs.

36 **Characterization**

37 Thermogravimetric analysis (TGA) was performed using the TA Q5000 instrument. The
38 sample was subject to a temperature ramp of 5 K/min under nitrogen flow.

1 Differential scanning calorimetry (DSC) measurements were performed using a TA Discovery
2 DSC series with liquid N₂ cooling. First, the samples were heated up from room temperature
3 to 350 K and then cooled down to 120 K. To allow full crystallization of the samples, *i.e.*, a
4 more reproducible thermal behavior, sub-ambient annealing was performed by thermal
5 cycling of the samples from 120 K to their cold crystallization temperature. Finally, the
6 samples were cycled between 120 K and 373 K two times with a ramp of 5 K/min. For both
7 TGA and DSC, the samples were filled in aluminum pans.

8 Density measurements were performed with an Anton Paar DMA 4500 M density meter.
9 Dynamic viscosity was determined with an Anton Paar MCR 102 rheometer, using a cone-
10 plate geometry with a shear rate of 10 s⁻¹. Both the density meter and the rheometer are
11 placed in a dry-room with a dew-point of 198 K.

12 The conductivity was determined in sealed glass conductivity cells (Materials Mates 192/K1)
13 equipped with two platinum electrodes (cell constant of (1.0±0.1 cm)) using a thermostatic
14 Bio-Logic conductivity meter.

15 Raman spectra were collected using the RAM II module of the Bruker Vertex 70v
16 spectrometer, mounting Nd:YAG laser source (1064 nm) and a high sensitivity InGaAs
17 detector. The samples were sealed in NMR tubes to prevent contamination. The signal was
18 accumulated over 500 scans for each sample.

19 Far infrared absorption spectra were acquired using a Michelson interferometer (IFS66 V/S
20 Bruker) working under low vacuum (2 mbar), equipped with a 6 μm thick mylar beam-splitter
21 and DTGS detector. A Hg discharge lamp was used as a radiation source. A drop of the sample
22 (30 μL) was incorporated between the Si windows of a commercial cell. The optical path
23 length of the radiation was adjusted at 25 μm by a mylar spacer placed between windows.
24 Reference spectra were collected without a spacer to avoid Fabry-Perot interference effects.
25 In order to maximize the signal-to-noise ratio, 128 interferograms were accumulated, and
26 their average was Fourier transformed using the Blackman-Harris apodization function
27 (actual resolution 4 cm⁻¹). The absorption spectra were calculated via the Lambert-Beer law
28 and pre-processed using the OPUS software.

29 Infrared spectra were collected with a Bruker Vertex 70v using a KBr beam-splitter and a
30 DLaTGS detector. The samples were collected in the Attenuated Total Reflection (ATR)
31 configuration on diamond crystals. The sample chamber was kept under vacuum (2 mbar)
32 during the measurements. To enhance the signal-to-noise ratio the spectra and the
33 background were collected 256 times and averaged.

34 All NMR spectra (¹H, ¹³C and ¹⁹F) were collected at 298 K with a 600 MHz JEOL ECZR
35 spectrometer using a 5 mm Royal probe equipped with a z gradient coil producing a
36 maximum gradient strength of 0.9 T m⁻¹. All samples reached thermal equilibrium before
37 measurement. NMR measurements were made in coaxial tubes. The inner tube contains a
38 deuterated solvent (required for lock) whereas the outer tube was filled with the
39 investigated samples, allowing for a good signal-to-noise ratio. The aqueous solution was
40 directly prepared in the NMR tube by diluting the pure acids (or TEA) to 0.1 mol L⁻¹ in D₂O.
41 The chemical shifts were referenced by setting to zero the standard chemicals, *i.e.*, TMS for
42 ¹H and ¹³C, CCl₃ for ¹⁹F.

1 Diffusion experiments on ^1H were acquired with a sequence characterized by encoding pulse
2 duration, Δ of 4 ms, a diffusion time of 0.3 s, and 8 nominal gradient amplitudes, g , ranging
3 from 80 to 800 mT m^{-1} chosen to give equal steps in gradient squared. DOSY experiments
4 were recorded in a range of temperatures within 298 K and 333 K with an interval of 5 K, and
5 all samples had reached equilibrium before measurement. Before performing DOSY
6 measurement, for each temperature, the 90-degree pulse has been measured.
7 Diffusion experiments on ^{19}F were acquired with a sequence characterized by encoding pulse
8 duration Δ of 5 ms, a diffusion time of 0.1 s, and 8 nominal gradient amplitudes, g , ranging
9 from 80 to 800 mT m^{-1} chosen to give equal steps in gradient squared. DOSY experiments
10 were recorded in a range of temperatures within 298 K and 333 K with an interval of 5 K, and
11 all samples had reached temperature equilibrium before measurement. Before performing
12 DOSY measurement, for each temperature, the 90-degree pulse has been measured.

13 **Computational details**

14 All computations were carried out using the Gaussian 09 program package[118] at B3LYP/6-
15 311++G** level of theory. Starting geometries were built with Avogadro[119]. The geometry
16 optimization was carried out before computing the intensities of vibrational frequencies. The
17 calculated frequencies were assigned with the help of the VEDA software[120]. No imaginary
18 frequencies were observed for any system, indicating the reaching of a real minimum of the
19 potential energy surface. To account for biases arising from vibrational anharmonicity and
20 rough treatment of electron correlation, a scale factor of 0.98 was employed to facilitate the
21 comparison with experimental data[100]. The energetics of the acid deprotonation was
22 studied through single-point energy at the same level of theory.

23 **AUTHOR INFORMATION**

24 **Corresponding Authors**

25 AM: alessandro.mariani@kit.edu;

26 SP: stefano.passerini@kit.edu

27 **Author Contributions**

28 All authors have given approval to the final version of the manuscript. AM and MB
29 contributed to the same extent to the manuscript by conceptualization, interpretation of the
30 results, and writing the manuscript. XG synthesized the PILs and collected DSC, TGA,
31 conductivity, and viscosity data. AN supervised the FIR experiments. BC and NB performed
32 ^1H and ^{13}C NMR measurements. RB and AB supervised the NMR experiments and
33 performed ^{19}F and PGSE NMR measurements. LG and SP edited the drafts and supervised
34 the project.

35 **Funding Sources**

36 This research is partially supported by the Bundes Ministerium für Wissenschaft und
37 Forschung (BMWFi) research grant "FZK 03ETB003A HiFi-PEFC".

1 **ACKNOWLEDGMENT**

2 AM gratefully acknowledges Ms. Chiara Giovannini for the graphics of the Table of Contents,
3 and Prof. Dr. Enrico Bodo, Dr. Francesca Leonelli, Dr. Ivana Hasa, Dr. Giovanni Appetecchi,
4 and Dr. Luigi Bencivenni for the fruitful discussion. AM, XG, and SP acknowledge the support
5 of the Helmholtz Association. LG acknowledges support from Regione Lazio, through
6 Progetto di Ricerca 85-2017-15125 according to LR 13/08. All the authors gratefully
7 acknowledge the reviewer for her/his valuable comments.

8 **ABBREVIATIONS**

9 ¹³C-NMR: carbon-13 nuclear magnetic resonance
10 ¹⁹F-NMR: fluorine-19 nuclear magnetic resonance
11 ¹H-NMR: proton nuclear magnetic resonance
12 AIL: aprotic ionic liquid
13 ATR: attenuated total reflection
14 CLC: Cheng-Li correction
15 DEMA: diethyl methyl amine
16 DEMATfO: diethyl methyl ammonium triflate
17 DFT: density functional theory
18 DOSY: diffusion ordered spectroscopy
19 DSC: differential scanning calorimetry
20 DTGA: differential thermal gravimetric analysis
21 DLaTGS: deuterated lanthanum α alanine doped triglycine sulfate
22 DTGS: deuterated triglycine sulfate
23 FD: formation degree
24 FIR: far-infrared
25 HAc: acetic acid
26 HB: hydrogen bond
27 HMS: methanesulfonic/mesylic acid
28 HTEA: triethylammonium
29 HTFA: trifluoroacetic acid
30 HTfO: trifluoromethanesulfonic/triflic acid
31 HTFSI: triflimidic acid
32 IL: ionic liquid
33 k_B : Boltzmann constant
34 KTFA: potassium trifluoroacetate
35 MIR: mid-infrared
36 MS: methanesulfonate/mesylate
37 MW: molecular weight
38 Nd:YAG: neodymium-doped yttrium aluminum garnet
39 NE: Nernst Einstein
40 NMR: nuclear magnetic resonance

1 PA: proton affinity
2 PGSE: pulsed gradient spin echo
3 PGSTE: pulse gradient stimulated echo
4 PIL: protic ionic liquid
5 pK_a : negative base-10 logarithm of the acid dissociation constant
6 ppm: parts per million
7 SER: Stokes-Einstein relationship
8 TA: thermal analysis
9 TEA: triethylamine
10 TEAMS: triethylammonium mesylate
11 TEATFA: triethylammonium trifluoroacetate
12 TEATfO: triethylammonium triflate
13 TEATFSI: triethylammonium bis (trifluoromethylsulfonyl) imide
14 TFA: trifluoroacetate
15 TfO: trifluoromethanesulfonate/triflate
16 TGA: thermal gravimetric analysis
17 TMS: tetramethyl silane
18 VEDA: vibrational energy distribution analysis
19 VTF: Vogel-Tamman-Fulcher

20

21 References

- 22 [1] T.L. Greaves, A. Weerawardena, I. Krodkiewska, C.J. Drummond, Protic Ionic Liquids: Physicochemical Properties and
23 Behavior as Amphiphile Self-Assembly Solvents, *J. Phys. Chem. B.* 112 (2008) 896–905. doi:10.1021/jp0767819.
24 [2] T.L. Greaves, C.J. Drummond, Protic Ionic Liquids: Evolving Structure–Property Relationships and Expanding Applications,
25 *Chem. Rev.* 115 (2015) 11379–11448. doi:10.1021/acs.chemrev.5b00158.
26 [3] A. Mariani, R. Caminiti, M. Campetella, L. Gontrani, Pressure-induced mesoscopic disorder in protic ionic liquids: first
27 computational study, *Phys. Chem. Chem. Phys.* 18 (2016) 2297–2302. doi:10.1039/C5CP06800B.
28 [4] T. Welton, Ionic liquids: a brief history, *Biophys. Rev.* 10 (2018) 691–706. doi:10.1007/s12551-018-0419-2.
29 [5] D. Yalcin, C.J. Drummond, T.L. Greaves, Solvation properties of protic ionic liquids and molecular solvents, *Phys. Chem.*
30 *Chem. Phys.* 22 (2019) 114–128. doi:10.1039/c9cp05711k.
31 [6] P. Walden, Ueber die Molekulargröße und elektrisches Leitfähigkeit einiger gazehmolzenen Salze, *Bull. Acad. Imper. Sci St.*
32 *Petersbg.* 8 (1914) 405–422.
33 [7] R.D. Rogers, K.R. Seddon, Ionic Liquids - Solvents of the Future?, *Science* (80-.). 302 (2003) 792–793.
34 doi:10.1126/science.1090313.
35 [8] F. Endres, S. Zein El Abedin, Air and water stable ionic liquids in physical chemistry, *Phys. Chem. Chem. Phys.* 8 (2006)
36 2101. doi:10.1039/b600519p.
37 [9] T.L. Greaves, C.J. Drummond, Protic ionic liquids: properties and applications., *Chem. Rev.* 108 (2008) 206–37.
38 doi:10.1021/cr068040u.
39 [10] N.V.N. V. Plechkova, K.R.K.R. Seddon, Applications of ionic liquids in the chemical industry, *Chem. Soc. Rev.* 37 (2008) 123–
40 150. doi:10.1039/B006677J.
41 [11] R. Hayes, G.G. Warr, R. Atkin, Structure and Nanostructure in Ionic Liquids, *Chem. Rev.* 115 (2015) 6357–6426.
42 doi:10.1021/cr500411q.
43 [12] X. Gao, A. Mariani, S. Jeong, X. Liu, X. Dou, M. Ding, A. Moretti, S. Passerini, Prototype rechargeable magnesium batteries
44 using ionic liquid electrolytes, *J. Power Sources.* 423 (2019) 52–59. doi:10.1016/j.jpowsour.2019.03.049.
45 [13] X. Gao, F. Wu, A. Mariani, S. Passerini, Concentrated Ionic-Liquid-Based Electrolytes for High-Voltage Lithium Batteries
46 with Improved Performance at Room Temperature, *ChemSusChem.* 12 (2019) 4185–4193. doi:10.1002/cssc.201901739.
47 [14] X. Gao, X. Liu, A. Mariani, G.A. Elia, M. Lechner, C. Streb, S. Passerini, Alkoxy-functionalized ionic liquid electrolytes:
48 understanding ionic coordination of calcium ion speciation for the rational design of calcium electrolytes, *Energy Environ.*
49 *Sci.* (2020). doi:10.1039/D0EE00831A.
50 [15] X. Mao, P. Brown, C. Červinka, G. Hazell, H. Li, Y. Ren, D. Chen, R. Atkin, J. Eastoe, I. Grillo, A.A.H.H. Padua, M.F. Costa
51 Gomes, T.A. Hatton, Self-assembled nanostructures in ionic liquids facilitate charge storage at electrified interfaces, *Nat.*

- 1 Mater. (2019). doi:10.1038/s41563-019-0449-6.
- 2 [16] J.-P. Belieres, C.A. Angell, Protic Ionic Liquids: Preparation, Characterization, and Proton Free Energy Level Representation
3 †, *J. Phys. Chem. B.* 111 (2007) 4926–4937. doi:10.1021/jp067589u.
- 4 [17] A. Idris, R. Vijayaraghavan, A.F. Patti, D.R. MacFarlane, Distillable Protic Ionic Liquids for Keratin Dissolution and Recovery,
5 *ACS Sustain. Chem. Eng.* 2 (2014) 1888–1894. doi:10.1021/sc500229a.
- 6 [18] R. Hayes, S. Imberti, G.G. Warr, R. Atkin, Pronounced sponge-like nanostructure in propylammonium nitrate., *Phys. Chem.*
7 *Chem. Phys.* 13 (2011) 13544. doi:10.1039/c1cp21080g.
- 8 [19] H. Ohno, Functional Design of Ionic Liquids, *Bull. Chem. Soc. Jpn.* 79 (2006) 1665–1680. doi:10.1246/bcsj.79.1665.
- 9 [20] K. Fumino, A. Wulf, R. Ludwig, The potential role of hydrogen bonding in aprotic and protic ionic liquids, *Phys. Chem.*
10 *Chem. Phys.* 11 (2009) 8790. doi:10.1039/b905634c.
- 11 [21] R. Hayes, S. Imberti, G.G. Warr, R. Atkin, How Water Dissolves in Protic Ionic Liquids, *Angew. Chemie Int. Ed.* 51 (2012)
12 7468–71. doi:10.1002/anie.201201973.
- 13 [22] H. Doi, X. Song, B. Minofar, R. Kanzaki, T. Takamuku, Y. Umebayashi, A new proton conductive liquid with no ions: Pseudo-
14 protic ionic liquids, *Chem. - A Eur. J.* 19 (2013) 11522–11526. doi:10.1002/chem.201302228.
- 15 [23] K. Fumino, V. Fossog, P. Stange, K. Wittler, W. Polet, R. Hempelmann, R. Ludwig, Ion Pairing in Protic Ionic Liquids Probed
16 by Far-Infrared Spectroscopy: Effects of Solvent Polarity and Temperature, *ChemPhysChem.* 15 (2014) 2604–2609.
17 doi:10.1002/cphc.201402205.
- 18 [24] H. Watanabe, T. Umecky, N. Arai, A. Nazet, T. Takamuku, K.R. Harris, Y. Kameda, R. Buchner, Y. Umebayashi, Possible
19 Proton Conduction Mechanism in Pseudo-Protic Ionic Liquids: A Concept of Specific Proton Conduction, *J. Phys. Chem. B.*
20 123 (2019) 6244–6252. doi:10.1021/acs.jpcc.9b03185.
- 21 [25] A.T. Nasrabadi, L.D. Gelb, Structural and Transport Properties of Tertiary Ammonium Triflate Ionic Liquids: A Molecular
22 Dynamics Study, *J. Phys. Chem. B.* 121 (2017) 1908–1921. doi:10.1021/acs.jpcc.6b12418.
- 23 [26] J. Ingenmey, S. Gehrke, B. Kirchner, How to Harvest Grotthuss Diffusion in Protic Ionic Liquid Electrolyte Systems,
24 *ChemSusChem.* 11 (2018) 1900–1910. doi:10.1002/cssc.201800436.
- 25 [27] K. Fumino, A. Wulf, R. Ludwig, Hydrogen Bonding in Protic Ionic Liquids: Reminiscent of Water, *Angew. Chemie Int. Ed.* 48
26 (2009) 3184–3186. doi:10.1002/anie.200806224.
- 27 [28] S. Menne, J. Pires, M. Anouti, A. Balducci, Protic ionic liquids as electrolytes for lithium-ion batteries, *Electrochem.*
28 *Commun.* 31 (2013) 39–41. doi:10.1016/j.elecom.2013.02.026.
- 29 [29] V.I. Pârvulescu, C. Hardacre, Catalysis in Ionic Liquids, *Chem. Rev.* 107 (2007) 2615–2665. doi:10.1021/cr050948h.
- 30 [30] A. Mariani, R. Caminiti, F. Ramondo, G. Salvitti, F. Mocci, L. Gontrani, Inhomogeneity in Ethylammonium Nitrate–
31 Acetonitrile Binary Mixtures: The Highest “Low q Excess” Reported to Date, *J. Phys. Chem. Lett.* 8 (2017) 3512–3522.
32 doi:10.1021/acs.jpcclett.7b01244.
- 33 [31] A. Mariani, R. Caminiti, L. Gontrani, Water and hexane in an ionic liquid: computational evidence of association under high
34 pressure, *Phys. Chem. Chem. Phys.* 19 (2017) 8661–8666. doi:10.1039/C6CP08450H.
- 35 [32] O. Russina, M. Macchiagodena, B. Kirchner, A. Mariani, B. Aoun, M. Russina, R. Caminiti, A. Triolo, Association in
36 ethylammonium nitrate–dimethyl sulfoxide mixtures: First structural and dynamical evidences, *J. Non. Cryst. Solids.* 407
37 (2015) 333–338. doi:10.1016/j.jnoncrysol.2014.08.051.
- 38 [33] A. Mariani, O. Russina, R. Caminiti, A. Triolo, Structural organization in a methanol:ethylammonium nitrate (1:4) mixture: A
39 joint X-ray/Neutron diffraction and computational study, *J. Mol. Liq.* 212 (2015) 947–956.
40 doi:10.1016/j.molliq.2015.10.054.
- 41 [34] A. Mariani, R. Dattani, R. Caminiti, L. Gontrani, Nanoscale Density Fluctuations in Ionic Liquid Binary Mixtures with
42 Nonamphiphilic Compounds: First Experimental Evidence, *J. Phys. Chem. B.* 120 (2016) 10540–10546.
43 doi:10.1021/acs.jpcc.6b07295.
- 44 [35] O. Russina, A. Mariani, R. Caminiti, A. Triolo, Structure of a Binary Mixture of Ethylammonium Nitrate and Methanol, *J.*
45 *Solution Chem.* 44 (2015) 669–685. doi:10.1007/s10953-015-0311-7.
- 46 [36] C.A. Angell, N. Byrne, J.-P. Belieres, Parallel Developments in Aprotic and Protic Ionic Liquids: Physical Chemistry and
47 Applications, *Acc. Chem. Res.* 40 (2007) 1228–1236. doi:10.1021/ar7001842.
- 48 [37] M. Martinez, Y. Molmeret, L. Cointeaux, C. Iojoiu, J.C. Leprêtre, N. El Kissi, P. Judeinstein, J.Y. Sanchez, Proton-conducting
49 ionic liquid-based Proton Exchange Membrane Fuel Cell membranes: The key role of ionomer-ionic liquid interaction, *J.*
50 *Power Sources.* 195 (2010) 5829–5839. doi:10.1016/j.jpowsour.2010.01.036.
- 51 [38] P. Attri, R. Bhatia, J. Gaur, B. Arora, A. Gupta, N. Kumar, E.H. Choi, Triethylammonium acetate ionic liquid assisted one-pot
52 synthesis of dihydropyrimidinones and evaluation of their antioxidant and antibacterial activities, *Arab. J. Chem.* 10 (2017)
53 206–214. doi:10.1016/j.arabjc.2014.05.007.
- 54 [39] J. Stoimenovski, E.I. Izgorodina, D.R. MacFarlane, Ionicity and proton transfer in protic ionic liquids, *Phys. Chem. Chem.*
55 *Phys.* 12 (2010) 10341. doi:10.1039/c0cp00239a.
- 56 [40] Y. Lv, Y. Guo, X. Luo, H. Li, Infrared spectroscopic study on chemical and phase equilibrium in triethylammonium acetate,
57 *Sci. China Chem.* 55 (2012) 1688–1694. doi:10.1007/s11426-012-4634-6.
- 58 [41] P. Berton, S.P. Kelley, H. Wang, R.D. Rogers, Elucidating the triethylammonium acetate system: Is it molecular or is it
59 ionic?, *J. Mol. Liq.* 269 (2018) 126–131. doi:10.1016/j.molliq.2018.08.006.

- 1 [42] E. Bodo, Structural Features of Triethylammonium Acetate through Molecular Dynamics, *Molecules*. 25 (2020) 1432.
2 doi:10.3390/molecules25061432.
- 3 [43] M. Shen, Y. Zhang, K. Chen, S. Che, J. Yao, H. Li, Ionicity of Protic Ionic Liquid: Quantitative Measurement by Spectroscopic
4 Methods, *J. Phys. Chem. B*. 121 (2017) 1372–1376. doi:10.1021/acs.jpcc.6b11624.
- 5 [44] S.K. Mann, S.P. Brown, D.R. MacFarlane, Structure Effects on the Ionicity of Protic Ionic Liquids, *ChemPhysChem*. 21 (2020)
6 1444–1454. doi:10.1002/cphc.202000242.
- 7 [45] A.T. Nasrabadi, L.D. Gelb, How Proton Transfer Equilibria Influence Ionic Liquid Properties: Molecular Simulations of
8 Alkylammonium Acetates, *J. Phys. Chem. B*. 122 (2018) 5961–5971. doi:10.1021/acs.jpcc.8b01631.
- 9 [46] D.R. MacFarlane, M. Forsyth, E.I. Izgorodina, A.P. Abbott, G. Annat, K. Fraser, On the concept of ionicity in ionic liquids,
10 *Phys. Chem. Chem. Phys.* 11 (2009) 4962. doi:10.1039/b900201d.
- 11 [47] O. Hollóczki, F. Malberg, T. Welton, B. Kirchner, On the origin of ionicity in ionic liquids. Ion pairing versus charge transfer,
12 *Phys. Chem. Chem. Phys.* 16 (2014) 16880–16890. doi:10.1039/C4CP01177E.
- 13 [48] B. Kirchner, F. Malberg, D.S. Firaha, O. Hollóczki, Ion pairing in ionic liquids, *J. Phys. Condens. Matter*. 27 (2015) 463002.
14 doi:10.1088/0953-8984/27/46/463002.
- 15 [49] T.I. Morrow, E.J. Maginn, Molecular Dynamics Study of the Ionic Liquid 1- n-Butyl-3-methylimidazolium
16 Hexafluorophosphate, *J. Phys. Chem. B*. 106 (2002) 12807–12813. doi:10.1021/jp0267003.
- 17 [50] F. Philippi, D. Rauber, M. Springborg, R. Hempelmann, Density Functional Theory Descriptors for Ionic Liquids and the
18 Charge-Transfer Interpretation of the Haven Ratio, *J. Phys. Chem. A*. 123 (2019) 851–861. doi:10.1021/acs.jpca.8b10827.
- 19 [51] T. Cremer, C. Kolbeck, K.R.J. Lovelock, N. Paape, R. Wölfel, P.S. Schulz, P. Wasserscheid, H. Weber, J. Thar, B. Kirchner, F.
20 Maier, H.-P. Steinrück, Towards a Molecular Understanding of Cation-Anion Interactions-Probing the Electronic Structure
21 of Imidazolium Ionic Liquids by NMR Spectroscopy, X-ray Photoelectron Spectroscopy and Theoretical Calculations, *Chem.*
22 *- A Eur. J.* 16 (2010) 9018–9033. doi:10.1002/chem.201001032.
- 23 [52] P. Stange, K. Fumino, R. Ludwig, Ion Speciation of Protic Ionic Liquids in Water: Transition from Contact to Solvent-
24 Separated Ion Pairs, *Angew. Chemie Int. Ed.* 52 (2013) 2990–2994. doi:10.1002/anie.201209609.
- 25 [53] K. Fumino, R. Ludwig, Analyzing the interaction energies between cation and anion in ionic liquids: The subtle balance
26 between Coulomb forces and hydrogen bonding, *J. Mol. Liq.* 192 (2014) 94–102. doi:10.1016/j.molliq.2013.07.009.
- 27 [54] K. Fumino, A.-M. Bónsa, B. Golub, D. Paschek, R. Ludwig, Non-Ideal Mixing Behaviour of Hydrogen Bonding in Mixtures of
28 Protic Ionic Liquids, *ChemPhysChem*. 16 (2015) 299–304. doi:10.1002/cphc.201402760.
- 29 [55] S.K. Davidowski, F. Thompson, W. Huang, M. Hasani, S.A. Amin, C.A. Angell, J.L. Yarger, NMR Characterization of Ionicity
30 and Transport Properties for a Series of Diethylmethylamine Based Protic Ionic Liquids, *J. Phys. Chem. B*. 120 (2016) 4279–
31 4285. doi:10.1021/acs.jpcc.6b01203.
- 32 [56] M. Hasani, S.A. Amin, J.L. Yarger, S.K. Davidowski, C.A. Angell, Proton Transfer and Ionicity: An 15 N NMR Study of Pyridine
33 Base Protonation, *J. Phys. Chem. B*. 123 (2019) 1815–1821. doi:10.1021/acs.jpcc.8b10632.
- 34 [57] R. KANZAKI, K. UCHIDA, X. SONG, Y. UMEBAYASHI, S. ISHIGURO, Acidity and Basicity of Aqueous Mixtures of a Protic Ionic
35 Liquid, Ethylammonium Nitrate, *Anal. Sci.* 24 (2008) 1347–1349. doi:10.2116/analsci.24.1347.
- 36 [58] R. Kanzaki, H. Doi, X. Song, S. Hara, S. Ishiguro, Y. Umebayashi, Acid–Base Property of N -Methylimidazolium-Based Protic
37 Ionic Liquids Depending on Anion, *J. Phys. Chem. B*. 116 (2012) 14146–14152. doi:10.1021/jp308477p.
- 38 [59] X. SONG, R. KANZAKI, S. ISHIGURO, Y. UMEBAYASHI, Physicochemical and Acid-base Properties of a Series of 2-
39 Hydroxyethylammonium-based Protic Ionic Liquids, *Anal. Sci.* 28 (2012) 469–474. doi:10.2116/analsci.28.469.
- 40 [60] R. Kanzaki, X. Song, Y. Umebayashi, S. Ishiguro, Thermodynamic Study of the Solvation States of Acid and Base in a Protic
41 Ionic Liquid, Ethylammonium Nitrate, and Its Aqueous Mixtures, *Chem. Lett.* 39 (2010) 578–579. doi:10.1246/cl.2010.578.
- 42 [61] K. Hashimoto, K. Fujii, M. Shibayama, Acid–base property of protic ionic liquid, 1-alkylimidazolium
43 bis(trifluoromethanesulfonyl)amide studied by potentiometric titration, *J. Mol. Liq.* 188 (2013) 143–147.
44 doi:10.1016/j.molliq.2013.08.023.
- 45 [62] J. Ingenmey, M. von Domaros, E. Perlt, S.P. Verevkin, B. Kirchner, Thermodynamics and proton activities of protic ionic
46 liquids with quantum cluster equilibrium theory, *J. Chem. Phys.* 148 (2018) 193822. doi:10.1063/1.5010791.
- 47 [63] C. Schreiner, S. Zugmann, R. Hartl, H.J. Gores, Fractional walden rule for ionic liquids: Examples from recent measurements
48 and a critique of the so-called ideal KCl line for the walden plot, *J. Chem. Eng. Data*. 55 (2010) 1784–1788.
49 doi:10.1021/je900878j.
- 50 [64] M. Yoshizawa, W. Xu, C.A. Angell, Ionic Liquids by Proton Transfer: Vapor Pressure, Conductivity, and the Relevance of Δp
51 K_a from Aqueous Solutions, *J. Am. Chem. Soc.* 125 (2003) 15411–15419. doi:10.1021/ja035783d.
- 52 [65] K.R. Harris, On the Use of the Angell–Walden Equation To Determine the “Ionicity” of Molten Salts and Ionic Liquids, *J.*
53 *Phys. Chem. B*. 123 (2019) 7014–7023. doi:10.1021/acs.jpcc.9b04443.
- 54 [66] J.E. Tanner, Use of the Stimulated Echo in NMR Diffusion Studies, *J. Chem. Phys.* 52 (1970) 2523–2526.
55 doi:10.1063/1.1673336.
- 56 [67] D.H. Wu, A.D. Chen, C.S. Johnson, An Improved Diffusion-Ordered Spectroscopy Experiment Incorporating Bipolar-
57 Gradient Pulses, *J. Magn. Reson. Ser. A*. 115 (1995) 260–264. doi:10.1006/jmra.1995.1176.
- 58 [68] S.H. Chung, R. Lopato, S.G. Greenbaum, H. Shirota, E.W. Castner, J.F. Wishart, Nuclear magnetic resonance study of the
59 dynamics of imidazolium ionic liquids with -CH₂Si(CH₃)₃ vs -CH₂C(CH₃)₃ substituents, *J. Phys. Chem. B*. 111 (2007) 4885–

- 1 4893. doi:10.1021/jp071755w.
- 2 [69] K. Hayamizu, Y. Aihara, H. Nakagawa, T. Nukuda, W.S. Price, Ionic Conduction and Ion Diffusion in Binary Room-
3 Temperature Ionic Liquids Composed of [emim][BF₄] and LiBF₄, *J. Phys. Chem. B.* 108 (2004) 19527–19532.
4 doi:10.1021/jp0476601.
- 5 [70] C.J.F. Solano, S. Jeremias, E. Paillard, D. Beljonne, R. Lazzaroni, A joint theoretical/experimental study of the structure,
6 dynamics, and Li⁺ transport in bis([tri]fluoro[methane]sulfonyl)imide [T]FSI-based ionic liquids, *J. Chem. Phys.* 139 (2013).
7 doi:10.1063/1.4813413.
- 8 [71] A. Mariani, M. Bonomo, B. Wu, B. Centrella, D. Dini, E.W. Castner, L. Gontrani, Intriguing transport dynamics of
9 ethylammonium nitrate–acetonitrile binary mixtures arising from nano-inhomogeneity, *Phys. Chem. Chem. Phys.* 19
10 (2017) 27212–27220. doi:10.1039/C7CP04592A.
- 11 [72] M. Campetella, A. Mariani, C. Sadun, B. Wu, E.W. Castner, L. Gontrani, Structure and dynamics of propylammonium
12 nitrate-acetonitrile mixtures: An intricate multi-scale system probed with experimental and theoretical techniques, *J.*
13 *Chem. Phys.* 148 (2018) 134507. doi:10.1063/1.5021868.
- 14 [73] G. Annat, D.R. MacFarlane, M. Forsyth, Transport properties in ionic liquids and ionic liquid mixtures: The challenges of
15 NMR pulsed field gradient diffusion measurements, *J. Phys. Chem. B.* 111 (2007) 9018–9024. doi:10.1021/jp072737h.
- 16 [74] J.L. Lebiga-Nebane, S.E. Rock, J. Franclemont, D. Roy, S. Krishnan, Thermophysical Properties and Proton Transport
17 Mechanisms of Trialkylammonium and 1-Alkyl-1 H-imidazol-3-ium Protic Ionic Liquids, *Ind. Eng. Chem. Res.* 51 (2012)
18 14084–14098. doi:10.1021/ie301687c.
- 19 [75] D.M. Jollie, P.G. Harrison, An in situ IR study of the thermal decomposition of trifluoroacetic acid, *J. Chem. Soc. Perkin*
20 *Trans. 2.* (1997) 1571–1575. doi:10.1039/a608233e.
- 21 [76] T. Burankova, R. Hempelmann, V. Fossog, J. Ollivier, T. Seydel, J.P. Embs, Proton Diffusivity in the Protic Ionic Liquid
22 Triethylammonium Triflate Probed by Quasielastic Neutron Scattering, *J. Phys. Chem. B.* 119 (2015) 10643–10651.
23 doi:10.1021/acs.jpcc.5b04000.
- 24 [77] M.S. Miran, H. Kinoshita, T. Yasuda, M.A.B.H. Susan, M. Watanabe, Physicochemical properties determined by ΔpK_a for
25 protic ionic liquids based on an organic super-strong base with various Brønsted acids, *Phys. Chem. Chem. Phys.* 14 (2012)
26 5178. doi:10.1039/c2cp00007e.
- 27 [78] P.K. Chhotaray, R.L. Gardas, Thermophysical properties of ammonium and hydroxylammonium protic ionic liquids, *J.*
28 *Chem. Thermodyn.* 72 (2014) 117–124. doi:10.1016/j.jct.2014.01.004.
- 29 [79] L.E. Shmukler, M.S. Gruzdev, N.O. Kudryakova, Y.A. Fadeeva, A.M. Kolker, L.P. Safonova, Thermal behavior and
30 electrochemistry of protic ionic liquids based on triethylamine with different acids, *RSC Adv.* 6 (2016) 109664–109671.
31 doi:10.1039/C6RA21360J.
- 32 [80] L.E. Shmukler, M.S. Gruzdev, N.O. Kudryakova, Y.A. Fadeeva, A.M. Kolker, L.P. Safonova, Triethylammonium-based protic
33 ionic liquids with sulfonic acids: Phase behavior and electrochemistry, *J. Mol. Liq.* 266 (2018) 139–146.
34 doi:10.1016/j.molliq.2018.06.059.
- 35 [81] G.L. Burrell, I.M. Burgar, F. Separovic, N.F. Dunlop, Preparation of protic ionic liquids with minimal water content and 15N
36 NMR study of proton transfer, *Phys. Chem. Chem. Phys.* 12 (2010) 1571. doi:10.1039/b921432a.
- 37 [82] C. Iojoiu, M. Martinez, M. Hanna, Y. Molmeret, L. Cointeaux, J.-C. Leprêtre, N. El Kissi, J. Guindet, P. Judeinstein, J.-Y.
38 Sanchez, PILS-based Nafion membranes: a route to high-temperature PEMFCs dedicated to electric and hybrid vehicles,
39 *Polym. Adv. Technol.* 19 (2008) 1406–1414. doi:10.1002/pat.1219.
- 40 [83] H. Nakamoto, M. Watanabe, Brønsted acid–base ionic liquids for fuel cell electrolytes, *Chem. Commun.* (2007) 2539–2541.
41 doi:10.1039/B618953A.
- 42 [84] C. Iojoiu, P. Judeinstein, J.Y. Sanchez, Ion transport in CLIP: Investigation through conductivity and NMR measurements,
43 *Electrochim. Acta.* 53 (2007) 1395–1403. doi:10.1016/j.electacta.2007.04.065.
- 44 [85] Y. Kohno, H. Ohno, Ionic liquid/water mixtures: from hostility to conciliation, *Chem. Commun.* 48 (2012) 7119.
45 doi:10.1039/c2cc31638b.
- 46 [86] C. Iojoiu, M. Hana, Y. Molmeret, M. Martinez, L. Cointeaux, N. El Kissi, J. Teles, J.C. Leprêtre, P. Judeinstein, J.Y. Sanchez,
47 ionic liquids and their hosting by polymers for HT-PEMFC Membranes, *Fuel Cells.* 10 (2010) 778–789.
48 doi:10.1002/face.201000026.
- 49 [87] J.A. Bautista-Martinez, L. Tang, J.-P. Belieres, R. Zeller, C.A. Angell, C. Friesen, Hydrogen Redox in Protic Ionic Liquids and a
50 Direct Measurement of Proton Thermodynamics, *J. Phys. Chem. C.* 113 (2009) 12586–12593. doi:10.1021/jp902762c.
- 51 [88] H. Mauser, A. Albert und E. P. Serjeant: Ionization Constants of Acids and Bases. 1. Auflage. Methuen & Co., London,
52 John Wiley Sons, New York 1962. 179 Seiten 8° und 9 Abbildungen im Text. Preis: 21/-s, Berichte Der Bunsengesellschaft
53 Für Phys. Chemie. 66 (1962) 882–882. doi:10.1002/BBPC.19620661025.
- 54 [89] J.A. Riddick, W.B. Bunger, T.K. Sakano, Organic Solvents: Physical Properties and Methods of Purification (Techniques of
55 Chemistry, Vol. II) John A. Riddick (Baton Rouge, La.) and William B. Bunger (Indiana State University, Terre Haute, Ind.)
56 Wiley-Interscience, New York/London/Sydney/Toronto, *J. Chromatogr. Sci.* 12 (1974) 38A–38A.
57 doi:10.1093/chromsci/12.2.38A-b.
- 58 [90] J.B. Milne, T.J. Parker, Dissociation constant of aqueous trifluoroacetic acid by cryoscopy and conductivity, *J. Solution*
59 *Chem.* 10 (1981) 479–487. doi:10.1007/BF00652082.

- 1 [91] A. Trummal, L. Lipping, I. Kaljurand, I.A. Koppel, I. Leito, Acidity of Strong Acids in Water and Dimethyl Sulfoxide, *J. Phys. Chem. A*. 120 (2016) 3663–3669. doi:10.1021/acs.jpca.6b02253.
- 2
- 3 [92] A.K. Chandra, A. Goursot, Calculation of proton affinities using density functional procedures: A critical study, *J. Phys. Chem.* 100 (1996) 11596–11599. doi:10.1021/jp9603750.
- 4
- 5 [93] P. Bonhôte, A.-P. Dias, M. Armand, N. Papageorgiou, K. Kalyanasundaram, M. Grätzel, Hydrophobic, Highly Conductive Ambient-Temperature Molten Salts, *Inorg. Chem.* 37 (1998) 166–166. doi:10.1021/ic971286k.
- 6
- 7 [94] A.P. Abbott, Model for the Conductivity of Ionic Liquids Based on an Infinite Dilution of Holes, *ChemPhysChem.* 6 (2005) 2502–2505. doi:10.1002/cphc.200500283.
- 8
- 9 [95] Y.H. Zhao, M.H. Abraham, A.M. Zissimos, Fast Calculation of van der Waals Volume as a Sum of Atomic and Bond Contributions and Its Application to Drug Compounds, *J. Org. Chem.* 68 (2003) 7368–7373. doi:10.1021/jo034808o.
- 10
- 11 [96] K. Fumino, S. Reimann, R. Ludwig, Probing molecular interaction in ionic liquids by low frequency spectroscopy: Coulomb energy, hydrogen bonding and dispersion forces, *Phys. Chem. Chem. Phys.* 16 (2014) 21903–21929. doi:10.1039/C4CP01476F.
- 12
- 13
- 14 [97] K. Fumino, V. Fossog, P. Stange, D. Paschek, R. Hempelmann, R. Ludwig, Controlling the Subtle Energy Balance in Protic Ionic Liquids: Dispersion Forces Compete with Hydrogen Bonds, *Angew. Chemie Int. Ed.* 54 (2015) 2792–2795. doi:10.1002/anie.201411509.
- 15
- 16
- 17 [98] K. Fumino, E. Reichert, K. Wittler, R. Hempelmann, R. Ludwig, Low-Frequency Vibrational Modes of Protic Molten Salts and Ionic Liquids: Detecting and Quantifying Hydrogen Bonds, *Angew. Chemie Int. Ed.* 51 (2012) 6236–6240. doi:10.1002/anie.201200508.
- 18
- 19
- 20 [99] A. Mariani, M. Campetella, C. Fasolato, M. Daniele, F. Capitani, L. Bencivenni, P. Postorino, S. Lupi, R. Caminiti, L. Gontrani, M. Campetella, C. Fasolato, F. Capitani, P. Postorino, C. Fasolato, M. Daniele, S. Lupi, R. Caminiti, F. Capitani, L. Bencivenni, P. Postorino, S. Lupi, R. Caminiti, L. Gontrani, A joint experimental and computational study on ethylammonium nitrate-ethylene glycol 1:1 mixture. Structural, kinetic, dynamic and spectroscopic properties, *J. Mol. Liq.* 226 (2017) 2–8. doi:10.1016/j.molliq.2016.08.043.
- 21
- 22
- 23
- 24
- 25 [100] V.H. Paschoal, L.F.O. Faria, M.C.C. Ribeiro, Vibrational Spectroscopy of Ionic Liquids, *Chem. Rev.* 117 (2017) 7053–7112. doi:10.1021/acs.chemrev.6b00461.
- 26
- 27 [101] V.N. Emel'yanenko, G. Boeck, S.P. Verevkin, R. Ludwig, Volatile times for the very first ionic liquid: Understanding the vapor pressures and enthalpies of vaporization of ethylammonium nitrate, *Chem. - A Eur. J.* 20 (2014) 11640–11645. doi:10.1002/chem.201403508.
- 28
- 29
- 30 [102] A.B. Patil, B.M. Bhanage, Assessing ionicity of protic ionic liquids by far IR spectroscopy, *J. Mol. Liq.* 252 (2018) 180–183. doi:10.1016/j.molliq.2017.12.131.
- 31
- 32 [103] G. Gamer, H. Wolff, Raman and infrared spectra of gaseous secondary aliphatic amines [(CH₃)₂NH, (CH₃)₂ND, (C₂H₅)₂NH and C₂H₅NHCH₃], *Spectrochim. Acta Part A Mol. Spectrosc.* 29 (1973) 129–137. doi:10.1016/0584-8539(73)80015-7.
- 33
- 34 [104] Triethylamine FTIR spectrum (<https://webbook.nist.gov/cgi/cbook.cgi?ID=C121448&Type=IR-SPEC&Index=1#IR-SPEC>), <https://webbook.nist.gov/cgi/cbook.cgi?ID=C121448&Type=IR-SPEC&Index=1#IR-SPEC>. (n.d.).
- 35
- 36 [105] C.P. Rosenau, B.J. Jelier, A.D. Gossert, A. Togni, Exposing the Origins of Irreproducibility in Fluorine NMR Spectroscopy, *Angew. Chemie - Int. Ed.* 57 (2018) 9528–9533. doi:10.1002/anie.201802620.
- 37
- 38 [106] T. Takamuku, Y. Kyoshoin, H. Noguchi, S. Kusano, T. Yamaguchi, Liquid Structure of Acetic Acid–Water and Trifluoroacetic Acid–Water Mixtures Studied by Large-Angle X-ray Scattering and NMR, *J. Phys. Chem. B.* 111 (2007) 9270–9280. doi:10.1021/jp0724976.
- 39
- 40
- 41 [107] A. Mariani, R. Caminiti, M. Campetella, L. Gontrani, Pressure-induced mesoscopic disorder in protic ionic liquids: first computational study, *Phys. Chem. Chem. Phys.* 18 (2016) 2297–2302. doi:10.1039/C5CP06800B.
- 42
- 43 [108] R. Hayes, S. Imberti, G.G. Warr, R. Atkin, Amphiphilicity determines nanostructure in protic ionic liquids, *Phys. Chem. Chem. Phys.* 13 (2011) 3237–3247. doi:10.1039/C0CP01137A.
- 44
- 45 [109] R. Atkin, G.G. Warr, The Smallest Amphiphiles: Nanostructure in Protic Room-Temperature Ionic Liquids with Short Alkyl Groups, *J. Phys. Chem. B.* 112 (2008) 4164–6. doi:10.1021/jp801190u.
- 46
- 47 [110] D. Pontoni, J. Haddad, M. Di Michiel, M. Deutsch, Self-segregated nanostructure in room temperature ionic liquids, *Soft Matter.* 13 (2017) 6947–6955. doi:10.1039/C7SM01464C.
- 48
- 49 [111] M. Brehm, H. Weber, M. Thomas, O. Hollóczki, B. Kirchner, Domain Analysis in Nanostructured Liquids: A Post-Molecular Dynamics Study at the Example of Ionic Liquids, *ChemPhysChem.* 16 (2015) 3271–3277. doi:10.1002/cphc.201500471.
- 50
- 51 [112] T.L. Greaves, D.F. Kennedy, N. Kirby, C.J. Drummond, Nanostructure changes in protic ionic liquids (PILs) through adding solutes and mixing PILs, *Phys. Chem. Chem. Phys.* 13 (2011) 13501. doi:10.1039/c1cp20496c.
- 52
- 53 [113] J.N.A. Canongia Lopes, A.A.H. Pádua, Nanostructural Organization in Ionic Liquids, *J. Phys. Chem. B.* 110 (2006) 3330–3335. doi:10.1021/jp056006y.
- 54
- 55 [114] O. Suárez-Iglesias, I. Medina, C. Pizarro, J.L. Bueno, On predicting self-diffusion coefficients from viscosity in gases and liquids, *Chem. Eng. Sci.* 62 (2007) 6499–6515. doi:10.1016/j.ces.2007.07.004.
- 56
- 57 [115] W. Hayduk, S.C. Cheng, Review of relation between diffusivity and solvent viscosity in dilute liquid solutions, *Chem. Eng. Sci.* 26 (1971) 635–646. doi:10.1016/0009-2509(71)86007-4.
- 58
- 59 [116] T. Köddermann, R. Ludwig, D. Paschek, On the validity of Stokes-Einstein and Stokes-Einstein-Debye relations in ionic

- 1 liquids and ionic-liquid mixtures, *ChemPhysChem*. 9 (2008) 1851–1858. doi:10.1002/cphc.200800102.
- 2 [117] M. Kar, N. V. Plechkova, K.R. Seddon, J.M. Pringle, D.R. MacFarlane, *Ionic Liquids – Further Progress on the Fundamental*
- 3 *Issues*, *Aust. J. Chem.* 72 (2019) 3. doi:10.1071/CH18541.
- 4 [118] M.J. Frisch, G.W. Trucks, H.B. Schlegel, G.E. Scuseria, M.A. Robb, J.R. Cheeseman, G. Scalmani, V. Barone, G.A. Petersson,
- 5 H. Nakatsuji, X. Li, M. Caricato, A. Marenich, J. Bloino, B.G. Janesko, R. Gomperts, B. Mennucci, H.P. Hratchian, J. V. Ort,
- 6 D.J. Fox, *Gaussian 09, Revision D.01*, (2009).
- 7 [119] M.D. Hanwell, D.E. Curtis, D.C. Lonie, T. Vandermeersch, E. Zurek, G.R. Hutchison, *Avogadro: an advanced semantic*
- 8 *chemical editor, visualization, and analysis platform*, *J. Cheminform.* 4 (2012) 17. doi:10.1186/1758-2946-4-17.
- 9 [120] M.H. Jamróz, *Vibrational Energy Distribution Analysis (VEDA): Scopes and limitations*, *Spectrochim. Acta Part A Mol.*
- 10 *Biomol. Spectrosc.* 114 (2013) 220–230. doi:10.1016/j.saa.2013.05.096.
- 11